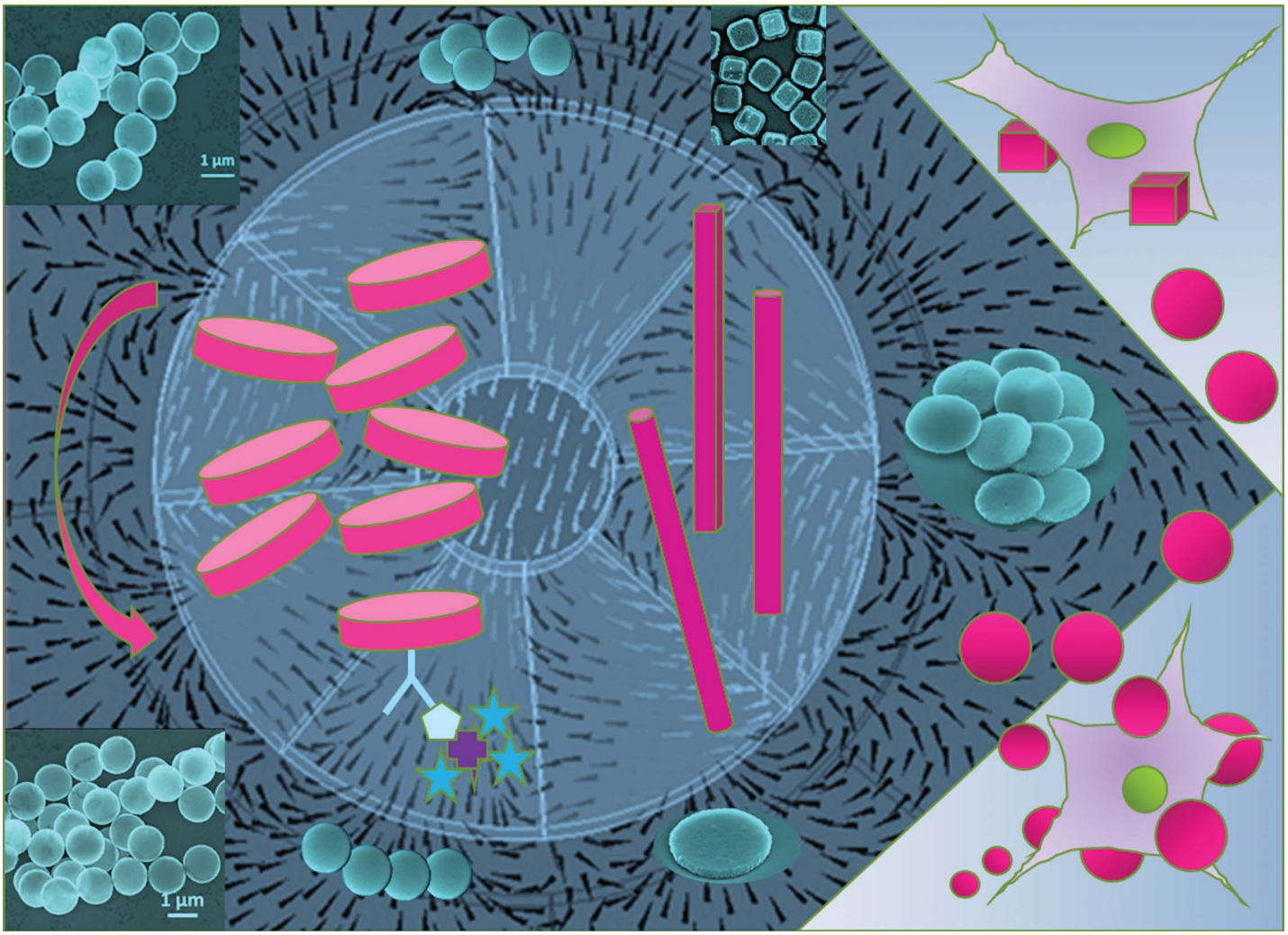

Showcasing research from SPINTEC, BrainTech Lab-INSERM and IRIG-SyMMES, CEA, CNRS, Univ. Grenoble Alpes, France.

Cancer treatment by magneto-mechanical effect of particles, a review

Triggering cancer cell death by low-frequency mechanical vibrations of magnetic nanoparticles - without heat production - is a growing field of research. This review shows the diversity of experimental studies, most *in vitro* and with the first *in vivo*, analyzing the impact of various types of magnetic particle and magnetic field sources. The effects of the local mechanical stress on cancer cells viability and tumor destruction are reported, potentially correlated with the cell perturbations and cell death pathways. This emerging bio-magneto-mechanical approach paves the way for new cancer treatments with reduced side effects.

As featured in:

See Cécile Naud, François Berger, Hélène Joisten *et al.*, *Nanoscale Adv.*, 2020, **2**, 3632.

ROYAL SOCIETY OF CHEMISTRY

rsc.li/nanoscale-advances

Registered charity number: 207890

Nanoscale Advances

ROYAL SOCIETY OF CHEMISTRY

REVIEW

View Article Online
View Journal | View Issue

Cite this: *Nanoscale Adv.*, 2020, **2**, 3632

Cancer treatment by magneto-mechanical effect of particles, a review

Cécile Naud,[ab] Caroline Thébault,[a] Marie Carrière,[c] Yanxia Hou,[c] Robert Morel,[a] François Berger,[b] Bernard Diény[a] and Hélène Joisten[*ad]

Received 5th March 2020
Accepted 19th June 2020

DOI: 10.1039/d0na00187b

rsc.li/nanoscale-advances

Cancer treatment by magneto-mechanical effect of particles (TMMEP) is a growing field of research. The principle of this technique is to apply a mechanical force on cancer cells in order to destroy them thanks to magnetic particles vibrations. For this purpose, magnetic particles are injected in the tumor or exposed to cancer cells and a low-frequency alternating magnetic field is applied. This therapeutic approach is quite new and a wide range of treatment parameters are explored to date, as described in the literature. This review explains the principle of the technique, summarizes the parameters used by the different groups and reports the main *in vitro* and *in vivo* results.

1. Introduction

Magnetic nano or micro particles have very attractive properties for biomedical applications.[1,2] So far, they have been widely studied and/or used for magnetic resonance imaging (MRI) as contrast agents,[3,4] magnetic targeting in particular for drug delivery[5,6] and sometimes in combination with MRI,[7] as part of the theranostics concept,[8] regenerative medicine,[9] cell sorting,[10] tissue engineering,[11] protein purification,[12] and for hyperthermia.[13–15]

Magnetic nano or microparticles are nano or micrometric sized materials with particular magnetic properties, which allow them to be remotely operated thanks to an externally applied magnetic field. They have a large surface-to-volume ratio, which is favorable to graft a large number of molecules onto their surface. It also promotes their interaction with biological entities such as cells, viruses, proteins and DNA.[16] Moreover, their magnetic properties can be modulated thanks to the shape and the composition of constitutive materials, so that they can be mechanically actuated, attracted to a region of interest, rotated, or used to generate a local heating. This is particularly interesting in the context of the expanding field of biomechanics, where they can be used to apply local forces or torques on biological specimens and to study the cellular response. Beside and in synergy with the classical modulation of molecular pathways using molecular medicine and/or targeted therapy, magneto-mechanical strategies should pave the way for new therapeutical strategies in the field of cancer. Targeted therapies modulate specifically specific molecular pathways involved in cancer such as proliferation, angiogenesis, cell death, invasion or immunosuppression for example. This has been a major biomedical progress. However, several limitations are emerging such as molecular resistances and relapse through molecular adaptation for heterogeneous tumor formations. Accessibility to the tumor microenvironment is also a major limitation. Magneto-mechanical therapies will not address a specific molecular target but will implement a specific physical action inside the tumor micro-environment providing new therapeutical opportunities. This new field of physics and medicine and biology will support a major inter-disciplinary work that is enlighten in this review.

The first uses of magnetic nanoparticles subjected to low-frequency alternating magnetic field to obtain a mechanical action on cells date back to 2008. Super Paramagnetic Iron-Oxide Nanoparticles (SPIONs) have been used to modify the intracellular calcium concentration of mast cells[17] or to activate the mechanosensitive TREK-1 receptor[18] involved in neuroprotection, epilepsy and depression, among others. In the same period, the interest of magnetic particles with shape anisotropy emerged, with the use of nickel nanowires to reduce the viability of fibroblasts.[19]

Considering the effects induced by low-frequency movements of magnetic particles and the possible mechanical effects of particles currently designed for hyperthermia,[20,21] a new technique to destroy cancer cells by low-frequency mechanical vibrations of magnetic particles was proposed and demonstrated in 2010.[22] The pioneering interdisciplinary study – involving nanomagnetism and biology – of Kim *et al.*, 2010,[22] likewise presented in the chapter of Novosad and Rozhkova, 2011,[23] highlighted this remarkable phenomenon of cancer cells destruction through the mechanical vibration of bio-functionalized magnetic vortex structures, which may lead, in

[a]*Univ. Grenoble Alpes, CEA, CNRS, Spintec, 38000 Grenoble, France. E-mail: helene.joisten@cea.fr*
[b]*BrainTech Lab, U1205, INSERM, Univ. Grenoble Alpes, CHU-Grenoble, France*
[c]*Univ. Grenoble Alpes, CEA, CNRS, IRIG-SyMMES, 38000 Grenoble, France*
[d]*Univ. Grenoble Alpes, CEA, LETI, 38000 Grenoble, France*

the longer term, to potential treatment of cancer with few sides effects. For the first time, a non-thermic mechanical force demonstrate its therapeutical effect. This promising approach gradually expanded over the last decade, as presented here. The most recent literature includes in particular the review of Goiriena-Goikoetxea *et al.*, 2020,[24] showing disk-shaped magnetic particles as magneto-mechanical actuator to destroy cancer cells, Chen *et al.*, 2020,[25] showing a magneto-mechanical approach based on nanocubes considered as nanospinner, and Maniotis *et al.*, 2019,[26] showing an alternating magnetic field source designed for the magneto-mechanical activation of particles. These articles emphasize the topicality and growing interest in this magneto-mechanical approach. In the present review, the principle of the treatment by magneto-mechanical effect of particles is explored. The different parameters which could be modulated are summarized, as well as the main *in vitro* and *in vivo* results presented in the literature. The perspectives for renewing our medical efficacy in cancer therapy are also summarized.

2. Presentation of cancer treatment by magneto-mechanical effect of particles

2.1 Principle

This method aims at inducing the cancer cell death or tumor destruction, by means of low-frequency mechanical vibrations of magnetic particles, with a very localized effect and thereby preserving the neighboring healthy cells. The induction of physical properties responding to the specific pattern of cancer cells and tissue is also an explanation for the specificity and safety of this approach. Like for chemotherapies or targeted therapies, the specific physics deregulation of cancer cells would explain the devoted effect of specific mechanical parameters on cancer cells. This relatively recent technique requires multidisciplinary expertise. In the literature, a multitude of terms can be found for it, including magnetolysis, magneto-mechanical actuation or stimulation therapy, magneto-actuation, non-chemo-toxic induction of cell death, mechanical tumor destruction, non-temperature induced effects, vibration or oscillations of magnetic particles by the application of a non-heating field that can be rotary or alternating at low frequency. This makes the review of the literature quite complex. For the rest of this article, we have chosen to use the term treatment by magneto-mechanical effect of particles (TMMEP), which refers both to the magnetic source of the stimulus and to the mechanical response of the particles that will act on cells.

Fundamental principle of the magneto-mechanical effect: the physical principle of the magneto-mechanical effect involved in "TMMEP" lies in the magnetic particles ability to be remotely actuated by an external magnetic field, in various configurations, as sketched in Fig. 1 and ref. 24 and 27. In an applied magnetic field **B** considered as uniform over the entire volume of the particle, the average magnetic moment $\mathcal{M}$ of the particle, which itself depends on the amplitude and direction of the applied field **B**, is subjected to the magnetic torque $\mathcal{M} \times \mathbf{B}$, and thus tends to align with the direction of the field. Meanwhile, if the magnetic anisotropy of the particle is high enough (exhibiting strong particle-composition, size, and shape dependence), the direction of the magnetic moment $\mathcal{M}$ remains almost blocked within the particle, parallel – or making a small angle – with the axis known as the easy axis of magnetization, or maintained in the easy plane of magnetization. On particles released or partially anchored in fluidic solutions, the effect of the magnetic torque becomes magneto-mechanical. It tends to re-orient the particle itself, until its easy axis or easy plane align with the applied magnetic field direction (like the earth's magnetic field effect on a compass needle). Rotating – or more generally variable – magnetic fields, spatially uniform, are thus used to induce continuous rotation or vibration of the particles in TMMEP. In this approach requiring effective magnetic torque, highly anisotropic particles are often preferred, such as for instance magnetic disks with "magnetic shape anisotropy",[24] or with "perpendicular magnetic anisotropy".[27]

Subjected to the variable magnetic field, the particle thus transfers its mechanical energy to its environment, on

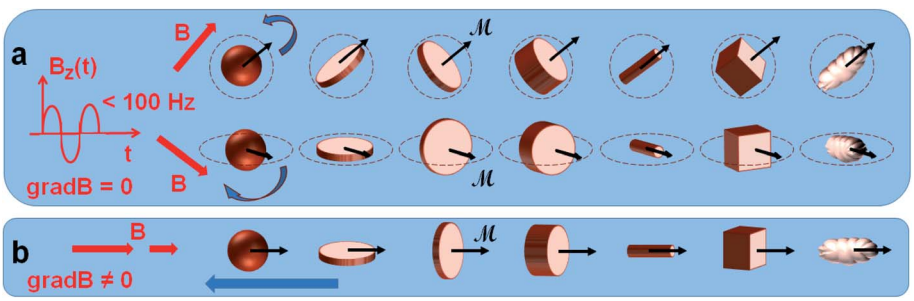

Fig. 1 Sketch of various types of magnetic particles exposed to variable magnetic fields, thus subjected to magneto-mechanical torques (and/or forces), tending to rotate (and/or translate) the particles. Average magnetic moment $\mathcal{M}$ of the particle: black arrows; applied magnetic field **B**: red arrows; particle rotation or translation direction: blue arrows. (a) Effect of the magnetic torque, generated by a spatially uniform magnetic field (grad**B** = 0), tending to align the magnetic moment $\mathcal{M}$ of the particle with the direction of the magnetic field **B**, leading to the particle rotation. $\mathcal{M} = \mathcal{M}(\mathbf{B})$. A rotating magnetic field can thus cause stable rotation or vibration of the particle, synchronized on its frequency (provided the frequency is low enough). (b) Magnetic force produced by the magnetic field gradient – derived from a spatially non-uniform magnetic field (*i.e.* grad**B** ≠ 0) – leading to the particle translation towards regions of large magnetic fields. Variable magnetic field gradient may also produce particle vibration.

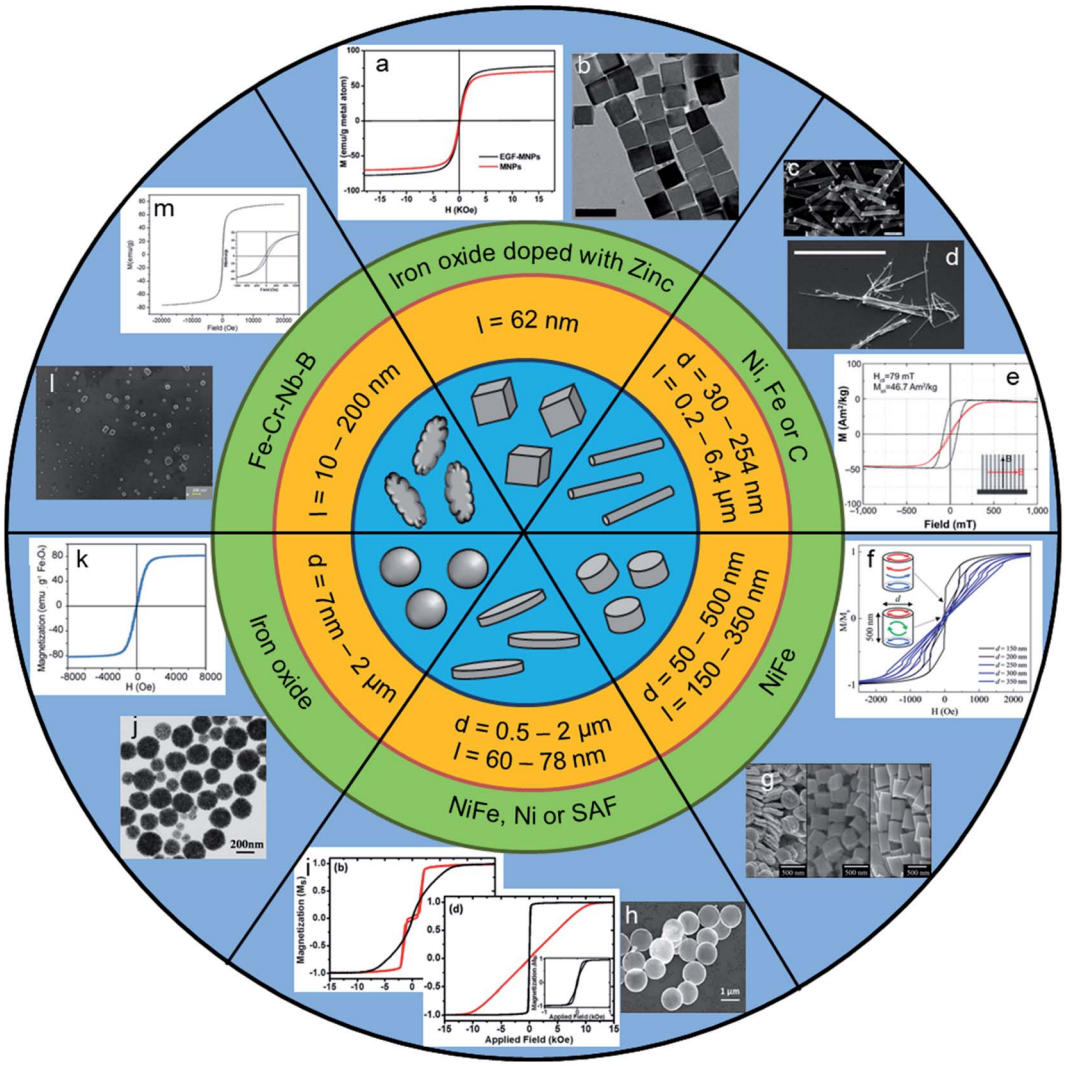

Fig. 2 Representative scheme showing properties of particles with different shapes, associated sizes and materials, and obtained results: microscopy images of particles and magnetization curves (magnetization as a function of magnetic field). Extracted from: (a and b) Shen *et al.*, 2017 (ref. 30) with (a) magnetization curve of dry particles at 300 K and (b) TEM images of iron oxide particles doped with zinc (l = 62 nm) [Reproducted with permission (ref. 30), Copyright© 2017, Ivyspring International Publisher, *Theranostics*]. (c) Kilinc *et al.*, 2015:[34] SEM image of Fe–Au nanorods (d = 254 nm and l = 2 μm) [Reproducted with permission (ref. 34), Copyright© 2015, Wiley-VCH, *Adv. Healthcare Mater.*]. (d) Martínez *et al.*, 2016:[35] SEM image of Fe nanowire (l = 6.4 ± 1.3 μm and d = 30–40 nm) [Reproducted with permission (ref. 35), Copyright© 2016, Springer Nature, *Sci. Rep.*]. (e) Contreras *et al.*, 2015:[33] magnetization loops of an array of Ni nanowires (l = 4 μm and d = 30–40 nm) with magnetic field applied in the in-plane (black) and out-of-plane (red) directions [Reproducted with permission (ref. 33), Copyright© 2015, Dove Press, *Int. J. Nanomed.*]. (f and g) Wong *et al.*, 2017 (ref. 36) with (f) hysteresis loop of NiFe particles with d = 150–350 nm (black to blue curve, respectively) and l = 500 nm, and (g) SEM images of NiFe particles of d = 350 nm and l = 75 nm, 200 nm and 500 nm (from left to right on the image) [Reproducted with permission (ref. 36), Copyright© 2017, Springer Nature, *Sci. Rep.*]. (h) Leulmi *et al.*, 2015:[38] SEM image of NiFe particles (d = 1.3 μm and l = 60 nm) [Reproducted with permission (ref. 38), Copyright© 2015, Royal Society of Chemistry, *Nanoscale*]. (i) Mansell *et al.*, 2017:[27] out-of-plane (red) and in-plane (black) hysteresis loops (b) for an array of 2 μm CoFeB/Pt particles and (d) for an array of 2 μm NiFe vortex particles [Reproducted with permission (ref. 27), Copyright© 2017, Springer Nature, *Sci. Rep.*]. (j) D. Cheng *et al.*, 2014:[32] TEM image of iron oxide particles (d = 200 ± 50 nm) [Reproducted with permission (ref. 32), Copyright© 2014, Springer, *Nanoscale Res. Lett.*]. (k) Wo *et al.*, 2016:[45] magnetization curve of hollow magnetic nanospheres of Fe_3O_4 (d = 250–550 nm) [Reproducted with permission (ref. 45), Copyright© 2016, Ivyspring International Publisher, *Theranostics*]. (l and m) Chiriac *et al.*, 2018 (ref. 52) with (l) SEM image and (m) magnetization curve of $Fe_{68.2}Cr_{11.5}Nb_{0.3}B_{20}$ particles (l = 10–200 nm) [Reproducted with permission (ref. 52), Copyright© 2018, Springer Nature, *Sci. Rep.*].

biological cells, in fluids or tissues. The frequency of the particle rotation or vibration is however limited to a few tens of Hz, the amplitude of mechanical vibrations decreasing sharply at higher frequencies owing to the viscosity of the fluid. The physical properties of the targeted tissue microenvironment will also impact the therapeutical response.

Furthermore, the magnetic forces generated on particles by a non-uniform field (*i.e.* through non-zero magnetic field gradient)[26] tend to move the particles in translation towards the regions of large field amplitudes. These forces can potentially be used to bring the particles towards targeted regions within a living organism.[28] Less effective in this approach than the

Table 1 Summary of particles properties, potential functionalization, and magnetic field sources, magnetic field amplitude, frequency and duration, and cancer cells properties, used in the literature for a TMMEP. Magnetic fields units (kA m^{-1}; Oe; G) reported as used in references and converted in SI unit (T or mT)[a,b,c]

Shape	References	Diameter	Length or thick-ness	Material	Functionalization	Chemo	Device	Field	Amplitude	Frequency	Duration	Cell line	Type[1]
Cube	Shen *et al.*, 2017 (ref. 30)	—	62 nm	Zn–IO[2]	DA–PAA–PEG + EGF peptide	—	Magnetic stirrer	Rotating	40 mT	15 Hz	30 min × 3 days	U87	Glioblastoma [A]
	Chen *et al.*, 2020 (ref. 25)	—	20 nm	Zn–IO[2]	TPP[3]	—	Magnetic stirrer	Rotating	40 mT	15 Hz	30 min	U87	Glioblastoma [A]
Nanowire	Fung *et al.*, 2008 (ref. 19)	200 nm	4.4 μm	Ni	—	—	Magnetic stirrer	Rotating	240 mT	1 Hz	20 min	NIH/3T3	Fibroblast
	Liu *et al.*, 2012 (ref. 31)	100 nm	1 μm	C+[4]	—	—	Magnetic stirrer	Rotating	40–75 mT	16.7 Hz	20 min	MCF-7	Breast cancer
	Wang *et al.*, 2013 (ref. 29)	80 nm	580 nm	Fe	Silica	—	Oscillating magnet	Oscillat. or Grad.	160 kA m^{-1} ~ 200 mT	2–10 Hz	20–60 min	HepG2	Hepatocellular carcinoma
	D. Cheng *et al.*, 2014 (ref. 32)	250–120 nm	200 nm	Fe_3O_4	—	—	Electro-magnet	Alternat.		35 kHz	0–10–30–60–120 min	HeLa[5]	Metastases [A]
	Contreras *et al.*, 2015 (ref. 33)	35 nm	4 μm	Ni	—	—	Coil	Alternat.	0.5 mT	1–1000 Hz	10–30 min	HCT116	Colorectal carcinoma
	Kilinc *et al.*, 2015 (ref. 34)	254 nm	1.98 μm	Fe–Au	PEG + HRG	Yes[6]	Electro-magnet	Alternat. + Grad.	—	0.5 Hz (1 s ON + 1 s OFF)	15 min	MCF7, MDA-MB-231	Breast cancer
	Martínez *et al.*, 2016 (ref. 35)	30–40 nm	6.4 μm	Fe	BSA, APTES	Yes[7]	Electro-magnet	Alternat.	1 mT	10 Hz	10 min	MDA-MB-231	Breast cancer
Cylinder	Wong *et al.*, 2017 (ref. 36)	150–350 nm	50–500 nm	NiFe	—	—	4 coils	DC, AC uni- or bi-axial pulsed	140 Oe = 14 mT	1–20 Hz	10 min	HeLa[4]	Metastases [A]
Disk	Kim *et al.*, 2010 (ref. 22)	1 μm	70 nm	Au/NiFe/Au	Anti-human-IL13a2R	—	Electro-magnet	Alternat.	90 Oe = 9 mT	10–60 Hz	10 min	N10	Glioma [A]
	Y. Cheng *et al.* 2015 (ref. 37)	2 μm	70 nm	Au/NiFe/Au	—	—	Halbach cylinder	Rotating	1 T	20 Hz	5–30 min	U87	Glioblastoma § [A]
	Leulmi *et al.*, 2015 (ref. 38)	1.3 μm	80 nm	Au/NiFe/Au	Anti-hCA9	—	Magnetic stirrer	Rotating	30 mT	20 Hz	45 min	SKRC59 hCA9	Renal carcinoma [A]
	Muroski *et al.*, 2016 (ref. 39)	2 μm	60 nm	SAF[8]	—	—	Halbach cylinder	Rotating	1 T	20 Hz	30 min × 3 days	HB1.F3.CD, U87	Neural stem cell, glioblastoma [A]
	Zamay *et al.* 2016 (ref. 40)	500 nm	60 nm	Au/Ni/Au	AS-9 et AS-14	—	Coil	Alternat.	100 Oe = 10 mT	100 Hz	10 min	EAC	Elrich cell[9] § [A]
	Mansell *et al.*, 2017 (ref. 27)	2 μm	118 nm, 70 nm	SAF[7] or Au/NiFe/Au	—	—	Halbach cylinder	Rotating	1 T	20 Hz	1 min	U87	Glioblastoma [A]

Table 1 (*Contd.*)

Shape	References	Diameter	Length or thick-ness	Material	Functionalization	Chemo	Device	Field	Amplitude	Frequency	Duration	Cell line	Type[1]
Sphere	Hu and Gao 2010 (ref. 41)	180 nm + 15 nm	—	Janus nano-composite + Fe_3O_4	PS_{16}-*b*-PAA_{10}	—	Magnetic stirrer	Rotating	—	0.83 Hz	15 min	LNCaP	Prostate tumor [A]
	Cho *et al.*, 2012 (ref. 42)	15 nm	—	Zn–IO	Ab for DR4	—	2 magnets	Grad.	0.2 T	—	2 h	DLD-1	Colon cancer § [A]
	Domenech *et al.*, 2013 (ref. 21)	61 ± 29 nm	—	Fe_3O_4	CMDx + EGF	—	Coil	Alternat.	42 kA m^{-1} ~ 52 mT	233 kHz	1 h	MDA-MB-23, 184-B5	Breast cancer, healthy mammary gland [A]
	Wang *et al.*, 2013 (ref. 29)	0.2–2 μm		Fe	APTES	—	Oscillating magnet	Oscillat. Or Grad.	160 kA m^{-1} ~ 200 mT	2–10 Hz	20–60 min	HepG2	Hepatocellular carcinoma
	D. Cheng *et al.*, 2014 (ref. 32)	200 nm	—	Fe_3O_4	—	—	Electro-magnet	Alternat.		35 kHz	0–10–30–60–120 min	HeLa[4]	Metastasis [A]
	E. Zhang *et al.*, 2014 (ref. 43)	0.1–5.8 μm	—	Fe_3O_4	Lamp-1	—	Coils	Alternat.+ Grad.	30 mT	5–20 Hz	20 min	INS1	Rat insulinome [A]
	Master *et al.*, 2016 (ref. 44)	7–8 nm	—	Fe_3O_4	PAA(PMA)–PEG ou PAA-P85	—	Electro-magnet	Alternat. Sinus.	50 or 100 kA m^{-1} ~ 62 or 125 mT	50 Hz	30 min or 3 × (10 min ON + 5 min OFF)	MDA-MB-231, BT474, MCF10A	Breast cancer, ductal carcinoma, healthy mammary gland
	Wo *et al.*, 2016 (ref. 45)	250–550 nm	—	Fe_3O_4	SiO_2/GQD + LB[10]	Yes[6]	4 moving magnets	Alternat.	45 mT	2000 rpm	20–60 min	Eca-109	Esophageal cancer cells
	Ju *et al.*, 2016 (ref. 46)	40 nm	—	Fe_3O_4	—	—	Coil	Alternat.	0.7 mT	100 Hz		HepG2, Bel-7402, HL-7702	Hepatocellular carcinoma[11], healthy hepatic cell [A]
	Brossel *et al.*, 2016 (ref. 47)	100 nm	—	Fe	—	—	2 magnets	Gradient	0.66 T	—	2 h × 21 days	MDA-MB-231	Breast cancer §
	Hapuarachchige *et al.*, 2016 (ref. 48)	80 nm	—	Fe_3O_4	Starch	—	MRI	Alternat. Grad. in bias high field	9.4 T	5.4 kHz	60 min	MDA-MB-231	Breast cancer
	Vegerhof *et al.*, 2016 (ref. 49)	50–100–200 nm	—	Fe_3O_4	PEG + C225	Yes[12]	Electro-magnet	Alternat.+ Grad.	6.2 G = 0.62 mT	4 Hz	15 min	A431	Skin cancer §
	Li *et al.*, 2017 (ref. 50)	30 nm	—	Fe_3O_4	DMSA	—	2 rotating magnets	Alternat.	0.1–20 mT	2–20 Hz	1 h	MCF-7	Breast cancer § [A]
	Lunov *et al.*, 2019 (ref. 51)	~60 nm	—	Fe_3O_4	Carboxy-dextran		Coil	High field pulses of 15 μs	5.5–8.5 T	~1.6 mHz	100 s	Huh7, Alexander, HepG2	Hepatocellular carcinoma, liver hepatoma, hepatoblastoma [A]

Table 1 (*Contd.*)

Shape	References	Diameter	Length or thick-ness	Material	Functionalization	Chemo	Device	Field	Amplitude	Frequency	Duration	Cell line	Type[1]
Anisotropic	Chiriac *et al.*, 2018 (ref. 52)	—	10–200 nm	Fe–Cr–Nb–B	—	—	4 coils	Rotating or Grad.	1–20 Oe = 0.1–2 mT	20–0–70–100 Hz	5–10–15–20 min	HOS, NHDF	Osteosarcoma, healthy skin cell ᴬ

[a] The § symbol is used to indicate *in vivo* studies; abbreviations: EGF: epidermal growth factor; Oscillat. = Oscillating; Grad. = Gradient; Alternat. = Alternating; Sinus. = Sinusoidal. [b] In the last column ("Type") of the present Table 1, ᴬ refers to "Apoptosis" mentioned as main cell death pathway, post-TMMEP, reported from the column 6 of Table 2. [c] [1] Human cells, except mentioned. [2] Zn–IO: iron oxide doped with zinc. [3] Triphenyl-phosphonium cation. [4] 5% metallic impurities. [5] Cervical cancer metastasis. [6] Vemurafenib. [7] Doxorubicin. [8] Synthetic antiferromagnet (SAF) composed of: Au/(Ta/Pt/CoFeB/Pt/Ru/Pt/CoFeB/Pt)/Au. [9] Mouse Ehlrich ascite adenocarcinoma. [10] Silica shell + graphene quantum dots + lipid bilayer. [11] Contamination by HeLa cells was recently demonstrated.[103] [12] Cetuximab.

torque effect, the gradient of a non-uniform magnetic field can likewise be used for generating the particles oscillations, through temporal variations of the field-gradient.[29] Particles being firstly rotated by the magnetic torque as a function of the field direction, the non-zero magnetic field gradient then guides the motion of particles.[26,28]

2.2 TMMEP parameters

For TMMEP, parameters such as shape, size and magnetic properties of the particles, frequency and amplitude of the applied magnetic field must be chosen in order to maximize the mechanical response of the particles within the biological tissue. As this technique is quite new and studied by groups with different backgrounds, there is a diversity in the parameters chosen by the different teams. A synthetic overview of the particle shapes, dimensions, compositions and magnetic properties, is presented in Fig. 2. Indeed, the type of particles and their functionalization, the applied field and the type of cancer cells greatly differ from one article to another, showing the extent of possibilities. Table 1 list the main parameters used in these studies, highlighting their heterogeneity.

2.2.1 Particle composition. Concerning the particles composition – presented in Table 1 – , the biocompatibility of their constitutive materials remains an essential point so that the particles can be used *in vivo* and then for clinical purposes. Biocompatibility is a mandatory prerequisite, that is often neglected in the *in vitro* studies. Integrating a specific exploration of biocompatibility implementing classical and regulatory test should be systematic before the initiation of large extensive studies, that will be never translated in absence of rigorous biocompatibility studies. Iron oxides such as magnetite (Fe_3O_4) or maghemite (γ-Fe_2O_3) are therefore very good candidates being usually chosen for their biocompatibility, although in some respects they may exhibit non-negligible cytotoxicity.[24,53,54] In particular, naked iron oxide nanoparticles are known to induce reactive oxygen species (ROS), considered as one of the main mechanisms of nanotoxicity, as investigated in Ling and Hyeon, 2013,[53] and Goiriena-Goikoetxea *et al.*, 2020.[24] However, this toxicity of iron oxide nanoparticles is greatly reduced when they are enveloped in a biocompatible layer, based either on inorganic shells, such as for example gold, silica or tantalum coatings, or on a large variety of biocompatible organic shells, depending on the nanoparticle core type and the intended applications.[53]

These materials were chosen by several groups.[21,29,32,41,43,44,48,51] However, in order to improve the magnetic actuation efficiency, larger magnetic susceptibilities than those of iron oxides may be required, in particular for low magnetic field operation. Magnetic materials such as nickel,[19,33] cobalt,[27,39] or NiFe alloys,[22,27,36,55] represent good alternatives. To ensure the biocompatibility of particles composed of these toxic metals,[56] limited dissolution should be ensured, for instance *via* a gold coating,[57,58] or polyelectrolytes.[59]

To specifically target a cell type or to increase the particle dispersion in fluids, surface functionalization of particles may be necessary.[60,61] Towards this goal, the deposition of a gold

layer on the particle surface allows the grafting of organic molecules through self-assembly of thiolates on the gold surface. These thiolates often have a polyethylene glycol (PEG) spacer and functional terminal groups. The PEG spacer increases particle stability, and the functional group allows the anchoring of biomolecules for specific targeting while providing biocompatibility.[62] The different surface ligands used in published studies are also presented in Table 1.

2.2.2 Particle size and shape. Among the wide range of magnetic particle types, manufactured from bottom-up or top-down approaches, the size and shape of the particles – depending on their composition – are largely variable. These physical parameters have a significant impact on the interaction with the biological environment, and on the TMMEP treatment itself. The particle size and shape must first be chosen to meet the basic requirements of biology, such as a sufficiently small size, and those of the TMMEP treatments, including an effective magneto-mechanical actuation and particles good dispersion in solution, as détailed below.

But first of all, physical properties of particles play a determining role not only in the effectiveness of the treatment and the particles behavior once they are in place, but also in their ability to target the tumor site, notably in case of intravenous injection. The impact of particles dimension and aspect ratio, when blood flow is used to transport them to the tumor site, is actively investigated. In particular Decuzzi *et al.*, 2010,[63] Albanese *et al.*, 2012,[64] and Ye, Shen and Li, 2018,[65] address the transport mechanisms in blood vessels as a function of particle size and shape; the global review of Wilhelm *et al.*, 2016,[66] moreover, analyses the delivery efficiency *versus* particle physical properties, and the fundamental limitations of particle doses (<1%) that can be delivered to tumors – see below in Section 4.[66] Ye, Shen, Yu *et al.*, 2018,[28] details the impact of nanoparticles size and shape in their "passive" or "active (subjected to magnetic forces for instance)" transport in the blood stream, in the area of drug delivery. The magneto-mechanical treatment TMMEP, similar in terms of tumor targeting, addresses the same issue of magnetic particles transport in blood flow, for potential clinical applications, as highlighted in the recent review Goiriena-Goikoetxea *et al.*, 2020.[24] These studies show that the particle shape – not only the size – clearly plays a key-role in the particle's ability to travel in the blood circulation.[24,28,66,67] Non-spherical particles, such as rods or discs, driven in the blood flow, exhibit a propensity to be more efficiently deflected towards the vessel wall, once they have escaped the macrophage uptake. This so-called phenomenon of margination, which consists in the particle lateral drift across the streamlines towards the endothelium, is favoured by an anisotropic shape of the particle, owing to inertial and hydrodynamical forces,[68] potentially enhanced by the magnetic actuation.[28] Spherical nanoparticles, being much more likely to follow the blood stream lines, however also marginate, as shown in Gentile *et al.*, 2008,[69] more efficiently for larger sizes. This expected phenomenon can lead to the particles adhesion on endothelium near the tumour site. The particles are then expected to diffuse from the blood vessel into the tumor tissue through the "leaky" vessel walls, and to be retained in the tumor site, based on the so-called "enhanced permeability and retention (EPR) effect" in tumor vasculature. The anisotropic shape of magnetic particle is again advantageous,[70] since generating oscillations due to hydrodynamic or magnetic forces, which leads to a stronger interaction of the particles with the vessel wall, and promotes their transmigration into the tumor.[24] The physical properties "size and shape" complemented with the "stiffness and surface functionality" of particles, so-called "4S" parameters,[28,65] are therefore decisive for the way particles circulate in the blood stream and penetrate the tumor.[28] However, intravenous injection of particles to target tumor sites remains challenging, for any particle shape and size,[66] as precised in Section 4.

A compromise is then required between a size that is small enough for *in vivo* use and large enough to achieve the intended magneto-mechanical effect on the cells. Indeed, the size of particles to be injected intravenously must be small enough not to clog the blood microcapillaries, thus to pass through the pores of blood vessels and to diffuse into tissues.[63,71] Moreover, for *in vivo* uses, particle size is limited by the injection device (to avoid needle clogging). Single SPIONs – fine spherical particles – are particularly appropriate for injections into biological samples, owing to their small sizes less than ~10–20 nm,[72] upper limit for achieving superparamagnetism in Fe_3O_4 nanoparticles. However, their low magnetic volume limits the magneto-mechanical effects. For a more effective magnetic actuation clustered SPIONs held by a ligand form particles of some 100 nanometers to a few micrometers in sizes.[73–75] Besides, the particles in recent studies composed of ferromagnetic layers, in the form of disks or pillars of diameters ranging from a few tens of nanometers to a few micrometers, have boosted studies on TMMEP. Producing larger magnetic forces or torques, such particles have been preferred to SPIONs clusters in various studies involving magnetic actuation on biological cells, despite more complex fabrication techniques.[22] The expected efficient actuation, very specific needs of this application in terms of mechanical transfer to the cells, can be fulfilled by these particles, owing to their anisotropic structures. Their potential shape anisotropy and perpendicular interfacial magnetic anisotropy have been used in TMMEP as cited below. Indeed, the magnetization remains quasi-blocked along the anisotropy direction, leading to an efficient mechanical actuation of the particles.

Secondly, combined to the magnetic actuation optimization, size and shape of the particles are chosen to achieve the particles redispersion in zero magnetic field, depending on the material used. Considering the magnetostatic interactions between particles, this property requires particles exhibiting zero or low remanence. Indeed, after their agglomeration in an applied magnetic field, suspended particles can get redispersed when the field is switched off, provided that their magnetic susceptibility remains below a certain threshold, as modelled in our ref. 76 illustrated in our ref. 55. This is particularly the case for SPIONs, which have zero remanence due to their small size yielding superparamagnetic properties, and smaller susceptibility than ferromagnetic particles. Low remanence can also be achieved by controlling the ferromagnetic particle shape and

size to obtain, for instance, disk-shaped particles exhibiting magnetic vortices.[22,27,77]

Finally, we observe for TMMEP various sizes and shapes of particles: from the spherical SPIONs of few nm in diameter,[44] the disk-shaped particles of few μm in diameter and few tens of nm in thickness, to the microrods of few μm in length. The sizes and shapes of the particles largely depend on the fabrication techniques, involving either bottom-up approaches (such as chemical routes, usually yielding quasi-spherical particles), or top-down approaches (such as microlithography techniques, usually yielding anisotropic particles, and allowing a wider freedom in the choice of the particles composition, size and shape). Each approach thus leads to specific magnetic and physical characteristics, and to particular experimental conditions in TMMEP, as mentioned here below.

Spheres. Although particles with a shape anisotropy are preferable to transfer a mechanical action on cells, several studies have observed a lethal effect on cancer cells by TMMEP using spherical particles.[43,44,46,49–51] It should be noted that such spherical particles may however form small chains due to their magnetostatic interactions in an applied magnetic field, and thus act as a unique elongated particle. The spherical particles used in TMMEP were mainly commercially available SPIONs fabricated by chemical routes, single or in cluster, actuated by applied magnetic fields of low frequency. Additionally, some studies aimed at inducing TMMEP with nanospheres, use either fields of higher frequencies (greater than 5 kHz),[21,32,48] or a static field gradient.[42,47] More complex structures are also explored to obtain anisotropic architectures, based on nanospheres assemblies. For instance, Hu and Gao developed Janus magnetic nanocomposite-particles, including SPIONs located in a single hemisphere of the particle to create a magnetic shape anisotropy.[41]

Disks (circles/squares basis). In addition to the spherical SPIONs widely studied in biomedical field for decades, recent disk-shaped particles composed of ferromagnetic layers, have emerged through the techniques of microelectronics, including photolithography and various deposition techniques such as sputtering, evaporation, or electrodeposition, in a top-down approach. They emerged for biological applications in 2008, consisting of synthetic antiferromagnetic (SAF) particles, exhibiting magnetization above those of SPIONs, zero remanence being achieved through the interlayer magnetic coupling, as firstly reported by Hu *et al.*, 2008.[78] The SAF structures consist of ferromagnetic multilayers, whose magnetizations are coupled antiparallel through non-magnetic spacer layer, such as ruthenium of thickness chosen in the range 0.6 nm to 0.9 nm. Particles with SAF configuration were firstly assessed as disk-shaped CoFe/Ru multilayers.[78] Furthermore, we investigated self-polarization and dispersion phenomena of SAF square-shaped particles, composed of NiFe/Ru multilayers.[76] Both SAF multilayers exhibit in-plane magnetization, while more recently, CoFeB/Pt-based SAF multilayers separated by Ru layers were chosen for their out of plane magnetization,[79] as outlined below.

In parallel, disk-shaped particles composed of permalloy monolayers (a nickel 80%–iron 20% alloy), exhibiting magnetic vortex configurations, have been investigated and explored to destroy glioma cells.[22,80] This innovative study proposed to induce cancer cells apoptosis (see in Section 3, below) through low-frequency vortex-disks vibrations (~20 Hz).[22] Fabricated by the top-down approach, such magnetic disks diameter and thickness have to be optimized to obtain the expected magnetic vortex configuration, as modelled by Guslienko *et al.*[77] This mainly in-plane magnetic structure, provides the expected low remanence and sufficient magnetic susceptibility for an effective magnetic actuation, while remaining below the critical threshold, preventing them from agglomeration.[36,55,76,81] This type of vortex-disk particles have been subsequently used in several studies to destroy several types of cancer cells, such as human renal carcinoma cells,[38] adenocarcinoma cells and glioblastoma cells.[39] They were also used for the first *in vivo* tests of TMMEP.[37]

The in-plane magnetized disk-shaped particles (SAF or vortex) may however present a theoretical issue, as highlighted by Mansell *et al.*,[27] since they could tend to orient with their plane in parallel to the plane of rotation of the field, if the surrounding environment permits it. In this hypothetical situation, if their plane is isotropic, magnetization may rotate within the particle plane without transferring mechanical energy to the surrounding environment, leaving the particle motionless. In contrast, when submitted to a rotating magnetic field, particles with out-of-plane magnetization indefinitely rotate with the field. Therefore, they are steadily able to transfer mechanical energy to the medium in which they are embedded.

In a previous study, disk-shaped particles with an out-of-plane SAF configuration were assessed,[79] magnetization being perpendicular to the plane of the multilayer interfaces. In good agreement with the hypothesis, a comparative experiment showed that SAF particles with perpendicular magnetization induced a stronger lethal effect on cancer cells than in-plane magnetized permalloy vortices, after the application of a rotating magnetic field for 1 min.[27]

Nanotubes. Nanowires or nanotubes have an improved shape anisotropy, which strongly tends to maintain their magnetic moment in parallel to the cylinder axis, and thus can yield an efficient magneto-mechanical actuation. The remanent magnetization on this easy axis may be close to 100% of their saturation magnetization M_s,[82] depending on the diameter/length ratio. This characteristic, however, leads to a potential aggregation of the particles after the exposure to the magnetic field. The first use of nanowires for a magneto-mechanical effect was tested on breast cancer cells.[31] In this study, carbon nanotubes contained 5% of metal impurities that gave the nanowires their magnetic properties. Clustering was observed when particles were subjected to the magnetic field. Moreover, Ni nanowires were used on colorectal carcinoma cells.[33] These particles are saturated in a field of less than 250 mT and have, as expected, a very high remanence (about 75% of M_s). Iron and iron oxide nanowires were also tested.[32,35] Wong *et al.*[36] studied influence of shape anisotropy, by varying length and diameter of cylindrical particles, from nanodisks to nanotubes shapes. These micromagnetic simulations result in a single vortex structure for particles of diameters ranging from 150 to 350 nm and less than 100 nm in length, in

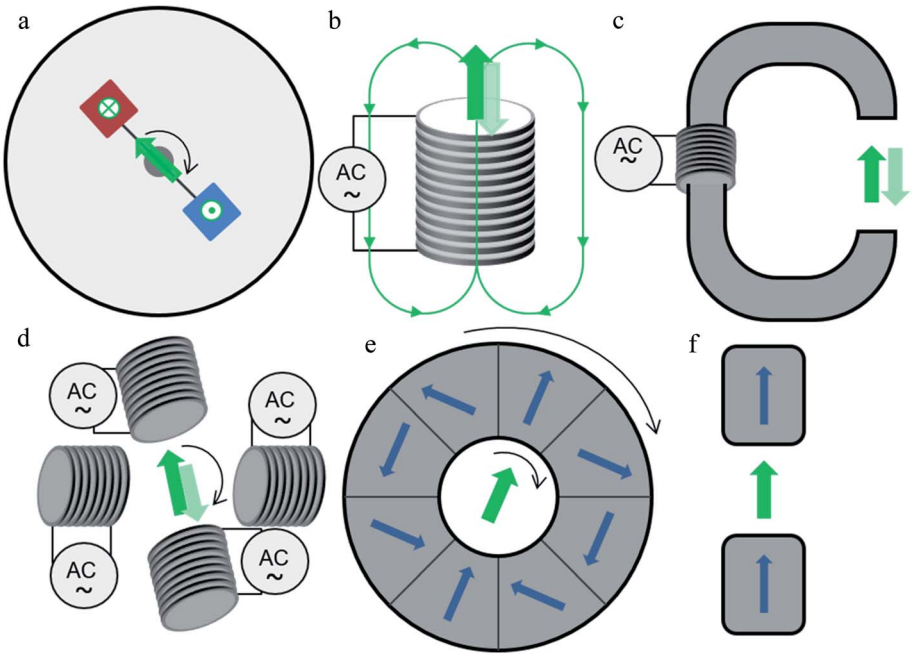

Fig. 3 Simplified diagrams of the mainly used magnetic field application devices. (a) Magnetic stirrer composed of two magnets at the end of a rotating rod (top view). (b) A coil powered by an alternating current that creates an alternating magnetic field inside or above the coil. The arrows in loops represent the magnetic flux line. (c) Ferrite core surrounded by a copper coil through which a sinusoidal alternating current flows. (d) System composed of 4 coils powered by an alternating sinusoidal current. The amplitude, phase shift and frequency of the applied current can be chosen to create an alternating or rotating field in the center of the 4 coils. (e) Halbach cylinder composed in this example of 8 permanent magnets creating an homogeneous field in the hollow of the cylinder. The rotating field is obtained by rotating the cylinder. (f) System composed of two magnets allowing to create a relatively homogeneous constant field.

accordance with the characteristics of disk-shaped particles. A double vortex structure appears for a length between 100 and 300 nm, which evolves to a triple vortex structure for lengths greater than 300 nm, a case close to nanowires.[36] A strong increase in susceptibility is observed for nanowire-shaped particles (d = 150 nm and l > 400 nm). However, the author[36] mentioned the contrast with ferromagnetic vortex discs usually known to show a reduction in susceptibility for a decrease in diameter or an increase in length,[77] as likewise experimented in our studies.[55,83] Nevertheless, this increase is here associated with an increase of remanence.[36] Calculations of the force applied to the cells show an induced force of the order of a few tens of pN for all diameters studied, sufficient to cause apoptosis of the cells (see in Section 3, below).[36] In a study comparing rod-shaped particles (d = 50–120 nm and l = 200 nm) with spherical particles (d = 200 nm) of iron oxides, the authors show better efficacy with rods.[32] Wang *et al.*[29] also compared rods (d = 80 nm and l = 580 nm) with spherical particles (d = 0.2–2 μm) and also observed a stronger effect with rods. This confirms the key role of the particle-shape anisotropy to transfer the mechanical torque provided by the external rotating or oscillating field to the cells. To allow two types of functionalization on the same particle, nanowires with a gold end were synthesized.[34] These particles combining two different surface properties are called Janus particles.

Cubes/spheres chains, and other anisotropic shapes. Although disks, spheres and nanowires are the three most commonly used forms of particles for TMMEP, cubic iron particles doped with zinc were also tested.[30] The authors observed an aggregation of chain-shaped particles during the application of the magnetic field, reducing the situation to the case of nanowire-shaped particles. In a similar approach, the nanochains formed by SPIONs subjected to a magnetic field are fixed by depositing a silica shell,[75] structures which, unlike nanowires, keep their superparamagnetic properties with a very low remanence. As a new approach, FeCrNbB particles produced by ball milling were used for TMMEP.[52] This manufacturing technique consists of grinding a metal powder to obtain anisotropic particles of nanometric size. The obtained size can be reduced between 10 and 200 nm. Besides, they exhibit low remanence and high susceptibility. The main disadvantage is a greater dispersion in size and less accurate control of particle properties. Purity of the initial powder and cleanliness of the manufacturing procedure are important to avoid contamination by other metals.

The systemic delivery also favors potential side effects because of the systemic exposition of the body. For these reasons, and because of the difficulties for a specific molecular targeting, local delivery is becoming the first emerging strategy.

2.2.3 Magnetic field. In order to induce a vibration or oscillation of the particles, the applied magnetic field must be rotating or alternating with a sufficient amplitude, preferably close to the saturation field of the particles. Alternatively, some groups explored the effect of static instead of oscillating

magneto-mechanical forces applied on cell membranes, in order to induce cell death, by the application of a constant magnetic field gradient on cell-bound particles.[42] Unlike hyperthermia, which requires high frequencies to induce heating (above 100 kHz to several MHz), TMMEP can be achieved at frequencies below 100 Hz.[22,31] As for particles characteristics, there is a wide variety of devices and applied magnetic field parameters (Table 1) for a TMMEP. A schematic representation of the different devices is shown in Fig. 3.

The first method of field application was to use commercial or homemade magnetic stirrers, traditionally used for stirring mixtures with a magnetic bar.[19,30,31,38] They are composed of two oppositely magnetized magnets located at each end of a rotating rod with the rotation speed up to 2000 rpm depending on the model (Fig. 3(a)). Advantage of these devices is that they are cheap and already present in most chemistry or biology laboratories. The major disadvantage is the inhomogeneity of the applied magnetic field. Indeed, a field mapping carried out on a commercial magnetic stirrer shows that right above the magnets, the field is perpendicular to the plane of the stirrer and has a value of 30 mT.[84] Although the term "rotating magnetic field" is generally used to refer to this type of device, the field acting on the particles located above the circular trajectory of the rotating magnets is actually pulsed up and down during the rotation of the magnets. Moving away from the trajectory by 1 cm outwards, the field strength decreases and an in-plane component appears, of about 5 mT. In the center of the agitator, the field is parallel to the plane and has a value of 15 mT, which is indeed a rotating field. In the rest of the literature, the field strength values applied with magnetic stirrer are given between 30 and 240 mT but the location of the measurement (center or above the trajectory of the magnets) is not indicated.[19,31,38,41,85] This device can only be used *in vitro*, taking care to distribute the cells to be treated over the path of the magnets for a pulsed vertical field, or in the center of the agitator for a rotating horizontal field. In both cases, the inhomogeneity of the field and the induced field gradient must be considered. Similarly, a system also based on the rotation of two magnets is used by Li *et al.*[50] In this case, the sample was placed between the ends of two rotating rods. The two rods were aligned and a magnet was placed at the end of each rod in opposite directions. The applied field was adjusted by varying the distance between the two rods with a maximum of 50 mT. Wo *et al.*[45] developed a more complex system using four permanent magnets placed on a disk under the culture plate producing a 45 mT field on the cells. During magnetic field exposure, the disk rotates and can also move on axial and radial direction.[45] Moreover, Maniotis *et al.*[26] recently developed a versatile system for TMMEP, configured with two to eight permanent magnets inserted in a rotating turntable, leading to field amplitudes of 200 mT and mean field gradient of 45 T m^{-1}.

A method widely used to apply an alternating magnetic field to cells consists in using coils or electromagnets (Fig. 3(b)–(d)). The field can be applied with an iron stick placed between the wells of a culture plate, itself wound with copper wire, to apply a 90 Oe (=9 mT) field.[22] Alternatively, the culture plate can be directly placed above a coil (Fig. 3(b)).[33,46,49,51] Kilinc *et al.*[34] used a Fe–Co–V tip wound with a copper coil to apply the magnetic field (the amplitude is not indicated).[34] In the latter case, the magnetic field was applied very locally (500 μm from the tip). Magnetic fields produced by these three methods are highly inhomogeneous and decrease sharply as a function of the distance from the field source. Another method consists in placing the sample in the air gap of a U or C-shaped ferrite core subjected to alternating current (Fig. 3(c)). This technique was chosen by D. Cheng *et al.*[32] and used at very high frequency (35 kHz) on cells detached from the support and placed in a tube; and by Martínez-Banderas *et al.*[35] to apply a 1 mT field at 10 Hz. With this method, the magnetic field is homogenous in the air gap but limitations come from the size of the device compared to the field amplitude. In a different approach, cells or mouse are placed directly in the center of the solenoid to apply a 100 Oe (=10 mT) field.[40] Here again, the field amplitude is very limited. Several commercial devices composed of an induction system with a ferromagnetic core or several coils have also been used.[21,43,44] The field produced by these three systems creates a gradient that is either used by some authors or avoided by positioning the cells with respect to the field source geometry. The use of coils of identical size and even number, placed around the area of interest, creates a fairly homogeneous field around the symmetry plane separating them. This is referred to as Helmholtz coils (Fig. 3(d)). This configuration was used to apply a 140 Oe (=14 mT) uni- or bi-axial pulsed field.[36] The disadvantage of this method is the rapid heating of the coils when a high current is applied, which requires a cooling system.

In order to produce a homogeneous field of larger amplitude, a Halbach cylinder can be used (Fig. 3(e)). This cylinder is composed of several permanent magnets (usually 8, 12 or 16) suitably oriented to produce a uniform magnetic field in the hollow of the cylinder. Using a rotation system, this cylinder was used to apply a rotating field in its center of about 1 T on cells, but also on mice.[25,27,37,39] This device allows stronger fields to be applied in a limited space. The field rotation frequency is determined by the cylinder rotating speed which can be adjusted as required and is only limited by mechanical constrains (motor, generator, mechanical and magnetic forces, magnets weight).

In an innovative approach, a preclinical MRI system was used to apply a pulsed gradient.[48] The main advantage of this method is its compatibility for subsequent clinical use, as MRI imaging systems are already widely used in hospitals. The field strength applied here is 9.4 T at a frequency of 5.4 kHz.

As mentioned above, while most of the studies discussed here focus on an oscillating or rotational motion of particles, some studies aimed solely at creating static forces pulling on the cell-membrane-bound particles, through the application of a static magnetic field gradient.[42,47] In this case, static magnetic field gradients are applied using two permanent magnets placed on either side of cells or mouse (Fig. 3(f)). The maximum field created is between 0.2 and 0.66 T. However, in a study comparing the effects of an oscillating field and a field gradient, the oscillating field showed a better efficacy.[29] The magnetic field of amplitude 160 kA m^{-1} (*i.e.* $\mathbf{B} \sim 200$ mT) was here applied

Table 2 Percentage of cancer cells viability after full treatment (particles + field), compared with particle incubation and no field applied (particles) or in untreated cells (control). For clarity reasons, the results have been extrapolated and are expressed here as a percentage of viability, except for the results in italics. In this case, the LDH release is normalized to 1 for healthy cells, and expressed as a function of this value for the other conditions. In the absence of positive control, it is not possible to calculate a percentage of viability. The symbol † is used to indicate trypan blue cell counts with a haemocytometer (with the reserve that particles may be counted as dead cells). The authors refer to Table 1 where the exposure conditions are detailed[a,b,c]

		Test 1				Test 2				Test 3				
References	Experiment conditions		Particles + field	Particles	Control		Particles + field	Particles	Control		Particles + field	Particles	Control	Main effects
Fung *et al.*, 2008 (ref. 19)		**MTT**	11%		100%									CK /—
Kim *et al.*, 2010 (ref. 22)		**LDH**	∼10%	∼90%										CM /A
Hu and Gao, 2010 (ref. 41)		**TB**	23%	99%	100%									CM /A
Liu *et al.*, 2012 (ref. 31)	75 mT	**TB †**	70%	92%	100%	**PI**	∼80%	∼98%		**LDH**	*×1.61*	*×0.9*	*×1*	CM & CL /—
	40 mT	**TB †**	83%	92%	100%	**PI**	∼83%	∼98%		**LDH**	*×1.87*	*×0.9*	*×1*	
Cho *et al.*, 2012 (ref. 42)		**CCK8**	∼48%	∼95%										CM /A
Wang *et al.*, 2013 (ref. 29)	Nanowire	**TB**	65–70%	∼95%										CM /Nr
	Sphere	**TB**	∼70%	>95%										
	NP + EGF	**Resaz.**	∼70%		100%									
	NP	**Resaz.**	∼120%		100%		Breast cancer							
Domenech *et al.*, 2013 (ref. 21)														LP /A
	NP + EGF	**Resaz.**	∼100%		100%									
	NP	**Resaz.**	∼100%		100%		Healthy cells							
E. Zhang *et al.*, 2014 (ref. 43)	NP function.	**7-AAD**	98%		100%									LP /A
	NP	**7-AAD**	99%		100%									
D. Cheng *et al.*, 2014 (ref. 32)	Rod 1 h	**TB**	∼76%	∼93%		**MTT**	∼70%	100%						CM /A
	Rod 2 h	**TB**	∼60%			**MTT**	∼70%							
	Sphere 1 h	**TB**	∼89%	∼95%		**MTT**	∼92%	100%						
	Sphere 2 h	**TB**	∼85%			**MTT**	∼88%							
Contreras *et al.*, 2015 (ref. 33)	1 kHz, 30 min	**MTT**	∼62%		100%	**LDH**	∼66%		∼88%					CM /Nr
	1 Hz, 30 min	**MTT**	∼67%			**LDH**	∼66%		∼88%					
Master *et al.*, 2016 (ref. 44)	Breast cancer	**MTT**	∼50%	∼95%										CK /—
	Breast cancer	**MTT**	∼25%	∼85–95%										
	Healthy cells	**MTT**	∼82%	∼95%										
Y. Cheng *et al.*, 2015 (ref. 37)		**MTT**	40%	80%	100%	**7-AAD**	∼10%							CM /A
Kilinc *et al.*, 2015 (ref. 34)	0.5 Hz	**Optical**	∼50%		∼97%									CM /—
Leulmi *et al.*, 2015 (ref. 38)		**TB †**	∼20%	—	100%									CM /A
Wo *et al.*, 2016 (ref. 45)	20 min	**Cell**	∼74%	100–105%										CM /—
	60 min	**Titer**	∼58%	100–105%										
Muroski *et al.*, 2016 (ref. 39)	NSC	**MTT**	25%	58%										CM /A, /CD
	Glioblastoma	**Lucif.**	∼37%		100%									
Martínez-Banderas *et al.*, 2016 (ref. 35)	NP + doxo.	**Resaz.**	∼27%	∼37%	∼100%									IC /—
	NP	**Resaz.**	∼65%	∼95%	∼100%									
Hapuarachchige *et al.*, 2016 (ref. 48)		**MTS**	∼73%	∼95–97%										IC /—, CD
Vegerhof *et al.*, 2016 (ref. 49)		**TB**	∼49%	—	100%									CM /Nr
Wong *et al.*, 2017 (ref. 36)	1–5 Hz	**TB †**	∼50%	—	∼87%	**Resaz.**	∼73%		100%	**BrEth**	∼60%		∼92%	CM /A
Li *et al.* 2017 (ref. 50)	20 Hz 20 mT	**MTT**	∼75%	>95%										CM /A
Mansell *et al.*, 2017 (ref. 27)	Vortex, 1 min	**TB**	∼88%		∼99%									CM, IC /A, Nr

Table 2 (*Contd.*)

References	Experiment conditions	Test 1	Particles + field	Particles	Control	Test 2	Particles + field	Particles	Control	Test 3	Particles + field	Particles	Control	Main effects
	SAF, 1 min	**TB**	~38%		~99%									
Shen *et al.*, 2017 (ref. 30)	Day 1	**CCK8**	~65%	~130%		**PI**	~43%	~98%	~98%					CM, LP /A, Nr
	Day 2	**CCK8**	~40%	~80%										
	Day 3	**CCK8**	~10%	~50%										
Chen *et al.*, 2020 (ref. 25)		**TB**	~30%	~80%	~100%									CM, LP, IC /A
	With AS-9 and AS-14	**TB**	~10%		~70%			Ascites						
	Without	**TB**	~35%		~70%									
Zamay *et al.*, 2016 (ref. 40)	With AS-9 and AS-14	**TB**	~70%		~80%			Hepatocytes						CM /A
	Without	**TB**	~60%		~80%									
Chiriac *et al.*, 2018 (ref. 52)	20 Hz, 20 min	**MTT**	~55%		~95%									CM, LP, IC /A
Lunov *et al.*, 2019 (ref. 51)	8 T 15 μs pulses	**WST-1**	~40%	~105%	~95%									LP /A
Ju *et al.*, 2016 (ref. 46)	Drug delivery + NPs 100 Hz	—												CM /A

[a] Abbreviations: TB: trypan blue; CCK8 = WST-8 assay; Resaz.: resazurin assay, Lucif.: luciferase assay. NP: nanoparticle. EGF: epidermal growth factor. [b] Mainly mentioned effects of TMMEP on cells: CM: cellular membrane perturbation, (through membrane-bound or internalized particles); LP: lysosome perturbation (including on lysosomal membrane); CK: cytoskeleton and cytoplasm perturbation; CL: cell lysis; IC: intracellular perturbation. [c] Potentially initiating cell death pathways, in particular: /A: apoptosis; /Nr: necrosis or membrane rupture (leakage); /—: cell death, undefined pathway; CD: cell detachment.

by a magnet moved alternatively away or closer to the sample to produce the oscillating field and field gradient.

3. Effects on cancer cells *in vitro*

The various methods described above aim at reducing the viability of cancer cells, focusing on various cancer types and cell lines as presented in Table 1; their efficacy was assessed *via* counting the number of viable cancer cells, through different techniques as described below (in Section 3.1). The main percentages of cancer cells viability, extracted from the reported studies, have been summarized in Table 2. Some experimental parameters, in particular the conditions of magnetic field application, have been analyzed below in Section 3.1, correlated with the reported viability results.

In addition, a number of these studies describe the biological mechanisms at the cell level that could explain the observed decrease in cancer cell viability. Depending on the targeted internal/external part of the cell, the mechanical stress may locally damage the cell membrane (compromising its integrity, modifying its permeability), or may cause internal disturbances in the cytoplasm, including in particular perturbations of the lysosomes or cytoskeleton, as noted in Table 2 column 6, and described below in Section 3.2.

In most cases, these perturbations on cells are correlated with the expected and experimentally observed cell death pathways, induced by TMMEP (see Section 3.3 and Table 2). Among the different forms of cell death, largely investigated over the last two decades,[86–88] apoptosis and necrosis cover a wide range of cellular processes, with however a full range of features from fully necrotic to fully apoptotic.[86] Apoptosis, – referred as "programmed cell death" or "cellular suicide" – potentially purely physiological in the absence of external perturbation, can also be triggered in response to external perturbations in the extra- or intracellular microenvironment.[86] It is worth remembering that the elimination of apoptotic cells, engulfed by phagocytes, generally takes place without any inflammatory response in tissues, while necrosis is well known to induce inflammatory reactions.[87,89] This regulated cell death represents one of the essential natural process maintaining homeostasis of healthy tissue or organisms.[86–88] By contrast, the apoptosis pathway is well known to be often defective in cancer cells, for which evading apoptosis is a factor promoting their proliferation.[90,91] Precisely here, most of the reported works show that TMMEP can trigger cancer cell death through apoptosis pathway, some of them through necrosis, as shown in Table 2 (column 6), and Section 3.3.

All these studies were conducted on two-dimensional *in vitro* cell models, except Lunov *et al.*,[51] who utilized 3D multicellular aggregates to assess TMMEP efficacy.

3.1 Cellular viability

3.1.1 Cancer cell viability assays. Different techniques can be used to evaluate cell viability. In the studies presented in this review, the following assays – referenced below and in Table 2 – have been used.

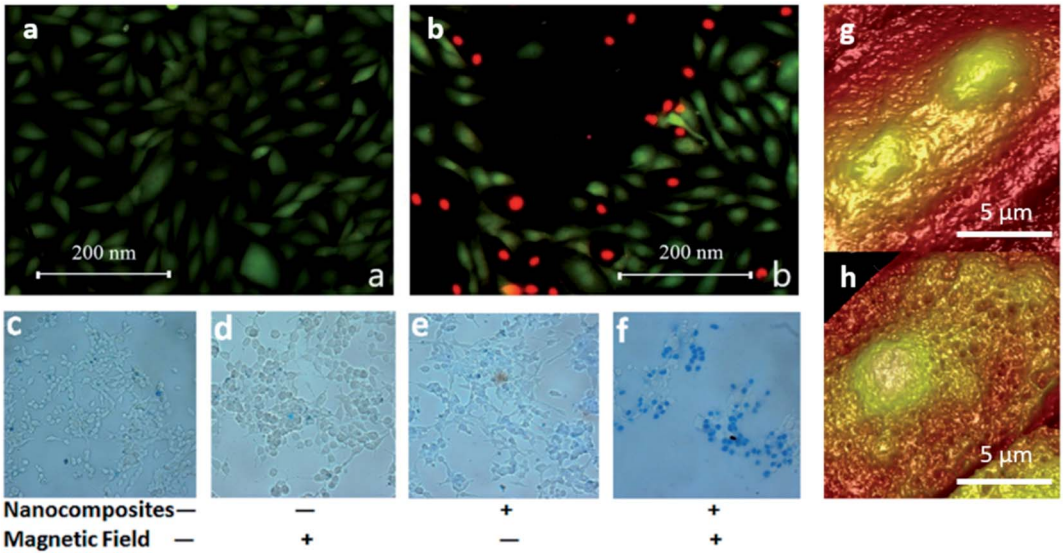

Fig. 4 (a) and (b) Extracted from Chiriac *et al.*, 2018:[52] human osteosarcoma cells (a) before and (b) after the magneto-mechanical actuation (rotating field). Live cells are colored in green and dead cells in red [Reproducted with permission (ref. 52), Copyright© 2018, Springer Nature, *Sci. Rep.*]; (c–f) extracted from Hu and Gao, 2010:[41] prostate cancer cells after treatment: (c) cells only, (d) cells exposed to magnetic field, (e) cells with particles, (f) cells with particles and exposed to magnetic field. Particles are biphasic iron oxide nanocomposites ($d = 180$ nm). Rotating magnetic field (0.83 Hz) was applied for 15 min. Dead cells appear blue due to trypan blue staining [Reproducted with permission (ref. 41), Copyright© 2010, American Chemical Society, *J. Am. Chem. Soc.*]; (g and h) extracted from Liu *et al.*, 2012:[31] cell membrane topographical imaging by AFM. (g) Control group. Surface of untreated cell was smooth. (h) MCF-7 cell treated by multiwalled carbon nanotubes exposed in 40 mT magnetic field for 20 min. Surface of the treated group is much rougher than controls with many small pore like structures [Reproducted with permission (ref. 31), Copyright© 2012, American Chemical Society, *Nano Lett.*].

- Assays based on the staining of dead cells: trypan blue (TB) is a cell permeant dye, which is released out of live cells. Live (non-colored) and dead (blue-colored) cells are then counted, manually under either a microscope, or automatically using a haemocytometer. This assay is distinguished from those where the dye enters only in dead cells: propidium iodide (IP), ethidium bromide (BrEth) and 7-AAD (7-aminoactinomycin D), which stain nuclei of cells that have lost their membrane integrity. These dyes are DNA/RNA intercalating agents, which become fluorescent upon intercalating. After incubation with the dye, the cell fluorescence is measured using flow cytometry.

- Assays evaluating the metabolic activity of cells: MTT (3-(4,5-dimethylthiazol-2-yl)-2,5-diphenyl tetrazolium bromide), WST-8 (2-(2-methoxy-4-nitrophenyl)-3-(4-nitrophenyl)-5-(2,4-disulfophenyl)-2*H*-tetrazolium), CCK8 (Cell Counting Kit) meaning WST-8 assay, WST-1 (4-[3-(4-iodophenyl)-2-(4-nitrophenyl)-2*H*-5-tetrazolio]-1,3-benzene disulfonate) and MTS (3-(4,5-dimethylthiazol-2-yl)-5-(3-carboxymethoxyphenyl)-2-(4-sulfophenyl)-2*H*-tetrazolium), are tetrazolium salts that are reduced by cellular NADH (nicotinamide adenine dinucleotide (NAD) in reduced form), forming formazan compounds that absorb light at specific wavelengths. The resazurin (Resaz.) assay (present for example in CellTiter-Blue® or PrestoBlue®) is reduced in metabolically-active cells into resorufin, which is pink and fluorescent.

- Assays based on the leakage of an enzyme from cells having impaired plasma membrane integrity, such as the LDH assay, in which the release of cytoplasmic LDH out of the cells is quantified after reacting with a tetrazolium salt.

- Assays combining two of these dyes, such as the LIVE/DEAD® test (*L*/*D*). It is based on the use of acetoxymethyl calcein (AM) which stains live cells and ethidium homodimer-1 (EthD-1) which stains dead cells. In metabolically-active cells, non-fluorescent calcein AM is converted by intracellular esterase activity to green fluorescent calcein. EthD-1 enters cells with impaired membranes and binds to nucleic acid, leading to red fluorescence.

In some studies, the number of live cells is quantified using optical microscopy and compared to the number of cells in untreated control. Some markers of the cell nuclei are also used, allowing to differentiate healthy cells from affected ones, which are characterized by dense nuclear staining and atypical shape.[34] Finally, the light intensity emitted by cells expressing luciferase is used in one study. This enzyme catalyzes bioluminescence reaction, it is used to quantify the number of cells.[39]

Some nanoparticles show interference with most of these assays. For instance, the presence of particles in cell cytoplasms impairs the appropriate counting of blue cells in the trypan blue assay when automatic counting is used. To use trypan blue for such application, cells should be manually counted under a microscope, taking care to differentiate between blue colored cells and particle charged cells that appear darker under the microscope. It has been shown that MTT, MTS, LDH and resazurin tests can interfere with some particles.[92,93] and that absorbance and fluorescence measurements can be affected by nanoparticles showing intrinsic absorbance or fluorescence property.[93] Therefore, when working with particles, the cell viability assay has to be carefully chosen so that interference is

minimal. It is recommended that several different toxicity assays should be implemented.

3.1.2 Cancer cell viability after TMMEP. Most studies show a decrease in cell viability following exposure to the magnetic field, as shown in Fig. 4. However, the order of magnitude is very different from one study to another. In some work the experimental conditions suggest that the particles might interfere with the assay, and appropriate controls are lacking. Moreover, under the same experimental conditions different groups sometimes show discrepant results. Finally, some results have been obtained only once, and should be reproduced before a final conclusion can be made. Consequently, the different studies summarized in this review should be compared with caution, because some of them are preliminary, while some others show statistically-significant results.

Results presented below show the lowest value of cell viability obtained, for each publication, when several conditions or parameters have been tested (Table 2).

Table 2 shows the wide variety of results obtained in the different published studies. Although not quantified, a significant decrease in cell viability after TMMEP was also observed with a 7-AAD test,[39] and a LIVE/DEAD test.[48]

In summary, no clear correlation between the observed effect and the used parameter can be derived from the comparison of these different studies. However, initial conclusions can be proposed, from some parameters tested, as described thereafter.

3.1.3 Influence of magnetic field characteristics, application time on cell viability

Influence of the field frequency on cell death. Most studies were carried out at low frequencies, between 10 and 50 Hz. A few studies have also tested very low frequencies between 0.5 and 5 Hz (see Table 1). These low frequencies are in contrast to the very high frequencies (above 1 kHz) used in some studies, which correspond to the frequencies commonly used for magnetic hyperthermia. These studies are cited here because the authors were interested in the induced mechanical effects and do not show any temperature increase during magnetic field application. In some work, the influence of magnetic field frequency on cell death induction was studied while keeping all other parameters constant. In the first study, conducted in 2010, the authors Kim *et al.*[22] showed that the optimal effect was obtained with frequencies of 10 and 20 Hz, inducing ~90% of cell mortality. The effect obtained was lower at 40 Hz (~75% of cell mortality), significantly decreased at 50 Hz (~25% of cell mortality) and non-existent at 60 Hz.[22] The effect of lower frequencies (from 1 to 20 Hz) was assessed by Wong *et al.*[36] in 2017, which showed a slight increase in lethal effect as the frequency decreases,[36] with ~80% of viable cells at 10 Hz and ~73% of viable cells at 1 Hz. However, these results contrast with those of Li *et al.*,[50] published in the same year, showing a better efficiency at 20 Hz, with 75% of cell viability, than at 2 Hz, with 80% of cell viability.[50] Similarly,Wang *et al.*[29] showed a better effect at 10 Hz compared to 2 and 5 Hz. Frequencies above 20 Hz were studied by Chiriac *et al.*,[52] in 2018. They showed a higher efficiency for a 50 Hz frequency with ~68% cell viability, compared to frequencies of 20, 70 and 100 Hz which gave cell viability of at least 75%.[52] In a study on colorectal cancer cells, a very low frequency (1 Hz) was compared to a much higher frequency (1 kHz), but with an applied magnetic field of only 0.5 mT while the particles saturation field is 250 mT.[33] The authors concluded that the efficiency is slightly better with a 1 kHz treatment with ~62% cell viability compared to ~67% of cell viability with a 1 Hz treatment, although this difference is not statistically significant. The similarity of the effect obtained with these two very different frequencies raises the question of the mechanisms involved. Indeed, it is possible that particles subjected to each frequency may be effective in causing a lethal effect, but through very different mechanisms.

Influence of the duration and repetition of magnetic field exposure. The magnetic field application duration varies from 1 min to 2 h and is sometimes repeated for several days (see Table 1). In a study published in 2015, a magnetic field of 20 Hz was applied *in vitro* for 5 or 30 min.[37] The authors showed an almost identical effect on cell viability after treatment (10.7% and 13% viability, respectively) with these two durations. In their *in vivo* study, the field was applied for 1 h and repeated daily during 1 week. In another *in vitro* study, a field of higher-frequency (35 kHz) and duration of treatment ranging from 10 to 120 min were used; the authors showed a greater decrease in cell viability with increasing exposure times, reaching 30% of decrease for 1 and 2 hours of treatment.[32] Similarly, a comparison between 10 and 30 min of treatment showed a better *in vitro* effect for 30 min,[33] although the best effect obtained was a 5% decrease in cell viability, which is rather low. Exposure times of less than 20 min were also tested,[49,52] and revealed a linear relationship between cell viability and exposure time. In conclusion, cell viability decreases with increased time of exposure to magnetic field. This effect seems to saturate beyond 1 hour of treatment.

By repeating the treatment daily (20 Hz field for 20 min), Zhang *et al.*[43] showed decrease of cell number compared to controls. However, it would be interesting to compare this result, obtained after repeated exposure, to the result that would be obtained after a single treatment. Similarly, Muroski *et al.*[39] showed a decrease in cell viability after three exposures to the magnetic field (20 Hz field for 30 min), but not compared to a single exposure.

A "pulsed" mode was also tested.[44] The magnetic field was applied for 10 min and then stopped for 5 min, with a total exposure time of 30 min. A higher decrease in cell viability was observed compared to continuous field application. Tested on two cell lines, cell viability decreased to ~25 and ~50% with pulsed mode *versus* ~50 and ~100% with continuous mode, for a particles concentration of 0.05 g L^{-1}.[44]

3.2 Targeted cancer cell components and cell activity affected by the treatment

3.2.1 Cellular membrane perturbation. Cell membrane alterations measured by the various tests presented above were directly observed in a study focusing on this aspect. Liu *et al.*[31] showed an increase in membrane roughness by Atomic Force Microscopy after application of a 75 mT magnetic field at 16.7 Hz for 20 min on cells exposed to nanowires, which was concomitant with an increase in membrane roughness, as

observed by Scanning Electron Microscopy,[31] and showed in Fig. 4(g) and (h). In an innovative approach, Muroski *et al.*[39] used neural stem cells (NSCs) as a vehicle to transport particles to cancer cells and then applied a rotating magnetic field to release the particles from NSC. After incubation time to let particles enter U87 cells, rotating magnetic field was applied to destroy U87 cancer cells. They observed that U87 cells were positively labelled with 7-AAD (unquantified) after only 30 s of field application (without NSC carrying).[39] Membrane integrity alteration was also reported by Wong *et al.*[36] in cells exposed to magnetic NiFe nanowires, and to a field of 140 Oe (*i.e.* 14 mT) at 1, 2 or 5 Hz for 10 min, *via* ethidium bromide staining.[36] The authors here hypothesized that membrane permeabilization was related to late apoptosis, which would need to be confirmed since no early apoptosis was detected.

3.2.2 Lysosomal perturbation. Lysosomes are cytoplasmic vesicles involved in several cellular processes and among them the hydrolysis of biomolecules and secretion of degradation products. The permeabilization of their membranes is regarded as a new strategy to induce cell death *via* the so-called lysosome-dependent pathway.[86] Playing an essential role in various programmed cell death pathways, lysosomes are notably involved in processes of apoptosis.[94,95] Several studies have focused on the impact of magnetically-actuated particles targeted to lysosomes. Domenech *et al.*[21] showed lysosomal membrane permeabilization (LMP) increase – through heat and/or mechanical damage – in 30% of cells treated with iron oxide magnetic particles targeted to the epidermal growth factor receptor, which were actuated *via* a 233 kHz magnetic field at a magnitude of 42 kA m^{-1} (*i.e.* ~52 mT), *via* acridine orange labelling. This treatment caused a 8% increase in the number of cells with lysosomal membrane rupture, assessed by monitoring cathepsin B activity,[21] cathepsins being proteolytic enzymes present in the lysosomal compartments that are released into the cytoplasm when lysosomal membrane is ruptured. This phenomenon was correlated with an increase in Reactive Oxygen Species (ROS, chemical species that cause oxidative stress on cells as their concentration increases) production after application of a very high frequency field.[21] In an approach specifically targeting lysosomes using the LAMP1 antibody, grafted onto SPIONS, Zhang *et al.*[43] also demonstrated a permeabilization of lysosomal compartments after applying a 30 mT field at 20 Hz for 20 min. Indeed, the intensity of the LysoTracker and LysoSensor Green markers decreased in this condition, as well as lysosome size. Lysosome disturbance was confirmed by Shen *et al.*[30] after 30 min of field application at 15 Hz on cells exposed to iron oxide nanoparticles doped with zinc, through galectin labelling and imaging by transmission electron microscopy, and by Lunov *et al.*[51] by studying acridine orange fluorescence. These authors also observed a reduction of mitochondrial membrane potential, mitochondrial dysfunction and ROS accumulation after LMP initiation.[51] However, in another study, Master *et al.*[44] found no evidence of lysosomal disturbance or LMP after the application of a 50 kA m^{-1} (*i.e.* ~62 mT) field at 50 Hz in pulsed mode (3 × 10 min) to cells exposed to superparamagnetic nanoparticles coated with block copolymers, which increases cell internalization and promotes clustering on lysosomes. In this study, LMP was assessed by labelling with LysoTracker Green and acridine orange.[44]

3.2.3 Cytoskeleton perturbation. The impact of the treatment on the cell cytoskeleton was studied with a particular focus on actin. When bound to ATP, this protein forms filaments that make up the skeleton of the cell.[90,96] A disturbance of the cytoskeleton was observed following the application of the magnetic field in the presence of particles.[44] Interestingly, the authors showed that lethal effect of the treatment depends on the mechanical properties of the cells. It explains why cancer cells, which are less rigid than healthy cells, are more affected by treatment. The use of cytochalasin D to reduce cell stiffness shows that healthy cells whose mechanical properties have been modified become vulnerable to mechanical stress induced by particle movement.[44]

3.2.4 Ionic exchanges. By measuring the electric current leaving cells, Ju *et al.*[46] showed that application of magnetic field, alone or in combination with magnetic particles, reduces the entry of anion into cells (reduction of about 40–43% for magnetic field alone and 54–57% for magnetic field with particles).[46] The effect is significantly weaker on healthy cells. Impact of mechanical particle stimulation on cellular ionic exchanges had already been observed.[17,18,97]

3.2.5 Overactivation of ERK proteins. Phosphorylation (addition of a phosphate group) of ERK (extracellular signal-regulated kinases) following the application of magnetic field in the presence of particles has been studied.[34] ERK proteins are kinases that activate other proteins by adding a phosphate group. An overactivation of these proteins causes the cell cycle to stop. The authors showed a higher phosphorylation of these proteins following treatment leading to cell death.

3.3 Main cell death pathways and processes observed in TMMEP

3.3.1 Apoptosis. Among the studies that have sought to determine the mechanisms involved in this magnetically-assisted cell death, the first hypothesis is that these treatments induce apoptosis in cancer cells. In 2010, Kim *et al.*[22] showed by a TUNEL test (terminal deoxynucleotidyl transferase dUTP nick end labelling) that 60% of cells (counted per 1000 cells on 6 wells) are positively labelled for apoptosis after local application of an AC field of 90 Oe (9 mT) at 20 Hz for 10 min.[22] TUNEL test is based on the enzyme TdT (terminal deoxynucleotidyl transferase) which recognizes the 3′-OH terminal groups released during DNA degradation. Similar results, although not quantified, were subsequently obtained in 2012 by Cho *et al.*[42] who showed, *via* immunostaining, the activation of caspase cascade, membrane inversion and blebbing after applying a continuous field of 0.2 T for 2 h, showing the onset of apoptosis. On the other hand, Zhang *et al.*,[43] who also assessed cell apoptosis post-treatment, showed that only ~7% of the cells underwent apoptosis after applying a 30 mT field at 20 Hz for 20 min, when using annexin V staining. They concluded that this apoptosis rate impacted cell proliferation.[43] In 2015,[37] cell apoptosis after the application of a 1 T field at 20 Hz for 5 min was studied by a TUNEL test. Number of positively labelled cells

Table 3 Summary of *in vivo* studies of the effectiveness of TMMEP. The "Model" column indicates the model chosen as well as the type and number of cells used for tumor induction. The "Particle injection" column first indicates the time of injection of the particles, defined as a day (Day 0 corresponding to tumor induction) or depending on the diameter D of the tumor; then indicates the quantity of particles injected as well as the injection procedure. The "Molecules" column indicates the complementary molecules used. The "Magnetic field" column indicates the first time of exposure, defined as a specific day or depending on the volume V of the tumor or a delay after NP injection. The duration of exposure to the field and possible repetitions are then indicated. The "Study" column indicates the time of sampling, often defined as a duration after magnetic field exposure (MFE) as well as the methods used to evaluate the effectiveness of the TMMEP. The abbreviation HE stands for hematoxylin–eosin labelling

		Particle injection			Magnetic field		Analysis	
Ref.	Model	Timing	Procedure	Molecule	Beginning	Duration	Timing	Procedure
Cho *et al.*, 2012 (ref. 42)	Zebrafish	Day 0	2.5 ng injected in the vitellus		24 h after NP	24 h	Immediately after MFE	Tail angle, apoptosis
Y. Cheng *et al.*, 2015 (ref. 37)	Athymic nude mice 1×10^5 U87 cells in orthotopic model (brain)	Day 0	50 NP/cell injected with cells		From day 4	1 h × 7 days	Along study	Survival study, tumor volume monitoring *via* luciferase
		Day 3	5×10^6 NP injected intra-tumoraly		From day 4	1 h × 7 days	Immediately after MFE	Apoptosis observation, HE label
Zamay *et al.*, 2016 (ref. 40)	ICR white mouse 1×10^6 EAC cells in the leg	Day 7	2×10^7 NP/100 μl PBS injected intra-tumoraly	AS-9 and AS-14	1 h after NP	10 min	4 h after MFE	HE label
Vegerhof *et al.*, 2016 (ref. 49)	Nude mice 2×10^6 A431 cells subcutaneous	$D > 4$–5 mm	6 mg of NP in 200 μl injected intravenously	Cetuximab	2 h after NP	30 min × 7 in 14 days	Week 3	Tumor volume monitoring
Brossel *et al.*, 2016 (ref. 47)	BALB/C mice 1×10^7 MDA-MB-231 cells subcutaneous	Day 0	5 mg of iron injected with cells		$V > 0.1$–0.2 cm^3	2 h × 21 days	Different timing	Tumor volume monitoring, HE label
Li *et al.*, 2017 (ref. 50)	C75BL/6 mice 1×10^5 MCF-7 cells subcutaneous	$D > 5$ mm	2 mg of NP (in average) injected subcutaneously		8 h after NP	1 h	24 h after MFE	HE label
M. Chen *et al.*, 2020 (ref. 25)	Athymic nude mice 5×10^6 U87 cells subcutaneous	Day 0, 2 and 4	5 mg kg^{-1} of NP injected intra-tumoraly		From day 1	30 min × 6 in 14 days	Day 21	Tumor volume monitoring, apoptosis observation, HE label
	Athymic nude mice 2×10^6 U87 cells in orthotopic model (brain)	Day 0	2.5 mg kg^{-1} of NP injected intra-tumoraly		From day 2	20 min × 5 days	Along study	Survival study, HE label

increases by about 30% after the application of the magnetic field. Also in 2015, Leulmi *et al.*[38] showed that the rate of apoptotic cells increased by 30% after the application of a 30 mT field at 20 Hz for 45 min, *via* annexin V staining and analysis by flow cytometry. Using the same technique, Shen *et al.*[30] observed in 2017 an increase of about 13% in the number of apoptotic cells after 30 min of application of the 40 mT field at 15 Hz.[30] In the recent study of Lunov *et al.*, 2019,[51] the treatment is based on application of short pulses of particularly high intensity magnetic field. Using an annexin V staining combined to caspase-3 activity evaluation, the authors show an increase of ~60% of apoptotic cells after TMMEP (percentage extracted from the Fig. 4(d) of ref. 51). The increase in apoptosis rate was also observed with 3D cellular multiaggregates.[51] Using two different markers (BCL-2, apoptosis-inhibiting protein and BAX, pro-apoptotic protein) and flow cytometry analysis, Ju *et al.*[46] showed that 18 to 22% of cancer cells were apoptotic after treatment, compared to 3% in a non-cancer cell line.[46] Application of magnetic field on cells that have not been exposed to particles also increases the number of apoptotic cells by up to 7%, in this study. This phenomenon was confirmed by western blot's analysis of the ratio of BCL-2 : BAX proteins that decreases after treatment, indicating a greater amount of pro-apoptotic proteins. Although not quantified, the presence of apoptotic cells was also confirmed by increased intensity of Hoechst 33258 staining of cell nuclei, probing chromatin condensation.[50]

3.3.2 Necrosis, cell membrane rupture. Instead of apoptosis, some of the studies obtained cancer cell necrosis as the main outcomes of the magneto-mechanical treatment. In particular, Wang *et al.*, 2013,[29] using either spindle-like iron particles or clusters of spherical nanoparticles (less efficient), induced necrosis through membrane damage of the HepG2 cancer cells, while the quick cell death excluded apoptosis pathway. Contreras *et al.*, 2015,[33] using magnetic nanowires, triggered cell membrane leakage revealing the membrane rupture, described as a non-apoptotic cell death mechanism. Vegerhof *et al.*, 2016,[49] using spherical magnetite nanoparticles, showed mechanical rupture of the cell membrane caused by particle vibration, and imaged by MRI *in vivo* necrosis in the tumor site.

3.3.3 Cells detachment. By optical microscopic observations, Hapuarachchige *et al.*[48] witnessed the detachment of cells from the bottom of the wells after combined exposure to magnetic iron oxide nanoparticles and magnetic field application. This phenomenon is also mentioned by Muroski *et al.*[39] on cells exposed to 2 μm multilayer magnetic disks and to a 1 T rotating magnetic field. The authors hypothesized that this detachment was due to cell death. Detachment of cells after treatment can be problematic for tests performed on bottom plate immediately after treatment. Indeed, detached cells would not be counted and analyzed. Moreover, since such an effect is specific to a 2D *in vitro* test, precautions should be taken while analyzing results.

3.4 Comments on the *in vitro* apoptotic occurrence in TMMEP

Clearly, whereas all treatments aim at minimizing the cell viability, the *in vitro* outcomes exhibit the great variability from one study to another (see Table 2). The diversity of the cellular responses can easily be understood, given the diversity of experimental conditions (Tables 1 and 2), as commented above.

Although without statistical validation, we can observe some trends based on all the *in vitro* studies. As shown in Table 2 (column 6), apoptosis represents, in most cases, the latest stage of the above cited cellular perturbations,[21,22,25,27,30,32,36–43,46,50–52] however with variable rates of cancer cells mortality (or viability). Some of the studies show the induction of necrosis only – such as necrotic membrane disruption, cell membrane leakage or cell lysis.[29,33,49] Other studies mention both apoptosis and necrosis as cell death pathway.[27,30] The cell death pathway may likewise remain unspecified, neither apoptotic nor necrotic,[19,31,34,35,44,45,48] opening the door to further studies.[19]

Concerning the influence of particle shape, studies using disc-shaped particle have all highlighted apoptotic pathways for the treated cancer cells (see in Table 1, noted "[A]" in the last column, and the viability percentage in Table 2). Several of the studies using spherical particles likewise observe apoptosis pathways, however not all of them. Nanorods have a greater propensity to induce necrosis, or more generally to induce more disruptive death pathway than apoptosis, such as membrane lysis.

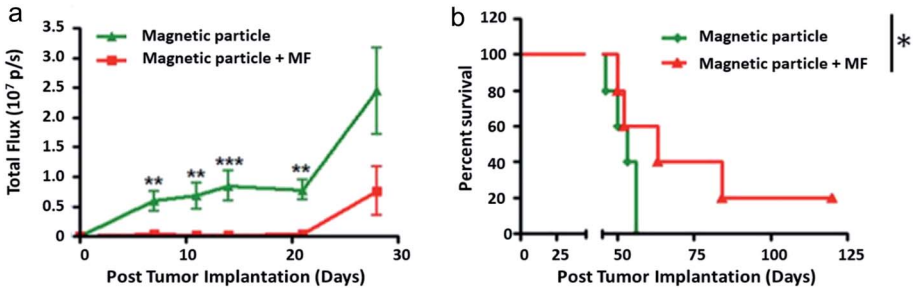

Fig. 5 Extracted from Y. Cheng *et al.*, 2015:[37] *in vivo* therapeutic efficacy of the magnetic particles (MPs) under rotating magnetic field. "The U87 cells were pre-incubated with MPs for 24 h and implanted in the mouse brain". (a) Quantification of the tumor bioluminescence signal over 4 weeks ($n = 5$ mice per group). Data are presented as mean ± SE. $^{**}p < 0.01$, $^{***}p < 0.001$ (Student's t test); (b) Kaplan–Meier survival curve of the mice with and without magnetic field treatment. $^{*}p < 0.05$ (log rank test) [Reproducted with permission (ref. 37), Copyright© 2015, Elsevier B.V., *J. Control. Release*].

Most published studies investigated classical molecular pathway as previously done for chemotherapy and targeted therapies. However, several groups recently described the existence of specific molecular pathway responding to mechanical forces. This open a new field of exploration that will be mandatory in the magneto-mechanical field – Broders-Bondon *et al.*, 2018.[98]

4. *In vivo* studies

Several groups studying TMMEP performed *in vivo* tests, a necessary step to validate the efficacy of this treatment. These studies are very important, when we integrate the major discrepancies observed between *in vitro* and *in vivo* efficacy in classical cancer therapies. This discrepancy might be much more important here, because of the major physical differences between liquid *in vitro* and the *in vivo* tissue microenvironment.

The tumor targeting, in living organisms, may be based either on a systemic injection (intravenous), or on a local injection of the particles within the tumor site. As indicated above in Section 2.2, anisotropic shapes of particles are much more suitable than nanospheres for their transport through the bloodstream.[24] However, considering potential clinical applications, intravenous administration of particles to target the tumor site remains challenging. The in-depth analysis of Wilhelm *et al.*, 2016,[66] shows the weak proportion of injected particles in the blood flow which penetrate the targeted tumor – less than 1%, so far – regardless of the particle shape and size. Biological mechanisms leading to the particles engulfment by phagocytic cells, which occur mainly in organs such as the liver, spleen and lungs,[63,66] highly contribute to eliminate particles from the blood circulation, preventing them to be delivered to the tumor site.[24,66] According to their size, particles may also be eliminated by the kidneys, lymph nodes and skin. Because of this systematic loss of particles, approaches utilizing a systemic administration of particles still require to be improved for clinical applications. The few TMMEP *in vivo* studies available in literature, presented in Table 3, show different modes of particles administration. The local injection of particles predominates – with two cases of particles previously mixed with the cancer cells for a common injection – leading to upstream level studies. One of them uses the intravenous mode, assuming that the tumor targeting and particles accumulation within the tumor site was helped by the EPR effect.[49] However, we can also consider that a direct injection of the magnetic particles into the tumor site is interesting for potential clinical applications. The TMMEP may then be the way to avoid the surgical removal of small tumors, or to act repeatedly after surgery on the remaining or recurrent cancer cells targeted by the particles.

The *in vivo* studies are summarized in Table 3. Details on particle material and field application were reviewed in Table 1.

In 2012, Cho *et al.*[42] studied the effect of applying a constant magnetic field of 0.5 T creating a gradient, for 24 h, on spherical zinc-doped iron oxide nanoparticles injected into zebrafish. Particles were functionalized to target the DR4 receptor (Death Receptor 4, which may be involved in triggering apoptosis) and were injected into the yolk at the embryonic stage. After magnetic field application, morphological alterations were observed in the tail, which had developed at an angle of 22°. Caspase 3 was studied here as a marker of apoptosis and a 6-fold increase in the number of caspase 3 positive cells was observed in zebrafish exposed to the magnetic field.[42]

The first *in vivo* rodent study was conducted by Y. Cheng *et al.*[37] on a mouse model of glioblastoma by orthotopic grafting (cancer cells were injected into their original organ, here the brain). The mice survival assay used magnetic particles incubated with the glioma cells prior to the tumor implantation. By applying a rotating field of 1 T at 20 Hz for 1 h daily for 1 week, the authors showed an increase in median survival from 56 days for the group exposed to particles without magnetic field application, to 63 days for the treated group with magnetic field, as shown in Fig. 5. Median survival for a group of control mice that would have been exposed neither to particles nor to the magnetic field is replaced here by mice submitted to particles only without field, the non toxicity and non efficiency of particles alone being verified. In this preliminary approach, vortex particles were injected at the same time as tumor cells and the field was applied from the 4th day post-implantation. Although anti-cancer treatments are usually tested from the 10th day, tumor size significantly increasing from this time.[99,100] Here, the authors[37] showed a significant decrease in tumor volume for 60% of mice on the day 28, using the fluorescence intensity of luciferase. To understand the involved mechanisms, a histological study was carried out on brain sections after a daily treatment of 30 min for 1 week, the particles being injected directly into the tumor on the 3rd day, *i.e.* 24 h before the beginning of exposure to the magnetic field. The authors[37] likewise showed a 19% increase in the number of cells in apoptosis. Almost all the particles are still located in the tumor 7 days after injection, and no particles have been found in other healthy organs (kidney, liver, lungs, large intestine, heart, bladder, spleen, testicles).

In a subcutaneous tumor model, Vegerhof *et al.*[49] showed significantly reduced tumor growth after application of a non-uniform field of 6.2 G (*i.e.* 0.62 mT) at 4 Hz for 30 min, repeated for 7 days.[49] The amplitude of the field is very small as compared to other published studies. Spherical magnetite particles of different sizes were injected intravenously about 2 hours before field application. Particles with a diameter of 200 nm functionalized with an antibody (cetuximab) to EGF receptors were most effective with a tumor growth of only 32% after 6 days of treatment compared to a growth of 548% for the particle-free control group with cetuximab injection alone. The hysteresis loops of particles could help in the understanding of the results.

Also in a subcutaneous model, Li *et al.*[50] observed morphological changes after the application of a magnetic field from 1 to 10 mT with a frequency varying between 2 and 20 Hz for 1 h. Spherical iron oxide particles were injected into the subcutaneous tumor and was exposed to the magnetic field 8 hours after injection. Euthanasia was performed 24 hours later and tissues were analyzed by a Hematoxylin–Eosin (HE) label that

allows the observation of cell morphology. The authors showed that tissues of control groups (saline injection and field exposure or particle injection alone) were normal while tissues subjected to particle injection and magnetic field appear destroyed. The effect was maximal at the highest frequency (20 Hz) as well as the highest field strength (20 mT).[50]

In vivo tests were also performed by Zamay *et al.*[40] by injecting adenocarcinoma cells into the mouse thigh. One hour after intra-tumor injection of the particles (nickel nanodiscs), mice were subjected to a field of 100 Oe (*i.e.* 10 mT) at 100 Hz for 10 min. Samples were collected 4 hours after the field application. Analysis of histological sections showed that injection of AS-9 and AS-14 aptamers lead to cancer cells destruction but that this effect was increased when the magnetic field is applied.[40] Monitoring tumor size by observing tumor pictures during treatment (injection of particles and/or aptamers + field application) repeated 3 times in 3 days showed that aptamers alone do not reduce the tumor volume. Application of magnetic field on non-functionalized particles caused destruction of the tumor but also of the muscles and epithelium, causing tissue necrosis. These phenomena are also visible after the field is applied to functionalized particles but appear from the 3rd day of treatment on the example shown here. In this type of assays, tumor and tissues imaging remains challenging.

In a different approach, the application of a field gradient was studied by Brossel *et al.*, 2016.[47] Iron nanoparticles were injected with cancer cells subcutaneously. A field gradient was applied from day 18 for 2 hours and repeated for 21 days. Authors showed a significant reduction in tumor volume compared to controls (median volume of 529 mm^3 for treated group *versus* 1334 mm^3 for control groups).

5. Discussion – summary

Although many advances have been made in the area of cancer therapy, the severe side effects of numerous treatments have oriented the research towards the development of targeted and local treatments. In particular, magnetic nanoparticles, already involved for decades in hyperthermia studies, recently show their strong potential to destroy cancer cells through their mechanical vibrations, remotely actuated by an alternating magnetic field at low frequency (a few tens of Hz). This review have identified and compared the studies, mostly *in vitro*, and the very first *in vivo* ones, focusing on this recent magneto-mechanical approach. Magnetic particles transfer very locally the energy of their mechanical vibration induced by the applied magnetic field, to the neighboring biological entities of micro- or nanometric dimensions. Studies reported here show the particles potential of destruction on different types of cancer cells in culture and in tumors (tested on a variety of cancer types such as glioblastoma, breast cancer, fibroblast, renal/hepatocellular/colorectal carcinoma, prostate tumor, insulinome, esophageal/skin cancer, osteosarcoma, *etc.*). The aim and ability of targeting malignant cells while sparing healthy ones is emphasized.

In most of the *in vivo* studies, magnetic particles are injected directly into the area of interest and therefore do not pass through the bloodstream. As long as the functionalization strategies for reaching the zone of interest are not sufficiently effective, it remains difficult to plan to inject the particles by venous route for potential clinical applications. Although venous injection remains a challenge for targeting the tumor, the size and especially the shape chosen for the particles – with the help of appropriate functionalization – could be determinant for their circulation in the blood flow, at least near the tumor site. Anisotropic shapes – nanodiscs or nanorods, nanowires – should be more favorable than the spherical ones, owing to the phenomenon of margination in the flow. Moreover, anisotropic particles penetrate more efficiently into the tumor site, owing to the EPR effect, increased if magnetically actuated by an alternative magnetic field. However, current studies are targeting particles administration directly into the tumor site.

Indeed, *in vivo* TMMEP studies remain currently limited to initial observations. To confirm the good preliminary results obtained *in vivo*, new study should be done, facing the problematic of particles injection and diffusion in the tumor. Moreover, three-dimensional cell culture models, as recently presented by (Lunov *et al.*, 2019),[51] as well as in our recent studies,[101,102] can advantageously mimic tumoral *in vivo* conditions, allowing to vary numerous relevant parameters.

The *in vitro* studies, although presenting highly variable experimental conditions, have allowed to test the behavior and efficiency of various types of particles. The particles of anisotropic shape turned out to exhibit advantages in different aspects of this approach. Favorable for the potential circulation in the blood stream, the anisotropic particles are likewise more efficient for converting magnetic forces or torques into mechanical effects on cells, leading to an efficient magneto-mechanical actuation. Furthermore, *in vitro* studies shows that depending on the particles anisotropic shapes – discs or elongated cylinders such as nanorods – , the occurrence of cell death pathway differs. Perturbations of the cellular membrane, the lysosome or the cytoskeleton in most cases led to apoptotic cell death pathway. However, necrosis without apoptosis was also reported. It can be noted that apoptosis is systematically reported in studies involving disk-shape particles, whereas nanorods or nanowires could be more destructive and potentially cause necrosis cell death. Spherical particles, such as SPIONs, likewise led to cancer cells destruction *via* apoptosis, as reported in two-thirds of studies using them. All these types of particles could however form small anisotropic chains or clusters when they are submitted to an applied magnetic field, leading to various shapes of magnetic microstructures acting on the biological cells.

Moreover, in terms of particles composition, ferromagnetic particles, since presenting higher magnetization than iron oxide nanoparticles, will exert larger forces or torques for a given magnetic volume. It may be noted that for any particle shape or composition, the cytotoxicity risks will have to be systematically assessed, since each type of particle has its own degre of toxicity, including SPIONS through ROS. Coating the particles with a biocompatible layer may be necessary, also allowing the bio-functionalization of particles. The particles

dispersion capability have been demonstrated for SPIONS as well as for ferromagnetic vortex particles, and for SAF particles under a threshold of magnetic susceptibility. Concerning the source of magnetic field, Halbach cylinder turned out to represent the magnetic field set-up providing the larger magnetic field remaining uniform in a rather large space. However for potential clinical applications, manufacturing Halbach cylinders with appropriate dimensions for treating the human body may be challenging. Other magnetic sources such as magnetic stirrer could thus be appropriate for TMMEP, despite a less uniform magnetic field.

The analysis of such studies firstly shows the growing interest in this magneto-mechanical approach, launched only ten years ago, initially published by Kim *et al.*, 2010.[22] The review reveals the great diversity of experimental conditions, and should yield a better assessments of certain cancer cell death parameters. The various type of magnetic micro–nanoparticles used in the different studies – their shapes, sizes, compositions, the resulting magnetic states and properties – the non-agglomeration requirements and the advantages of magnetic anisotropy for an efficient mechanical actuation, have been detailed. Likewise, the various available sources of alternative magnetic fields or field gradient have been presented.

In summary, TMMEP (cancer treatment by magneto-mechanical effect of particles) is based on a mechanical impact on cells induced by magnetic particles movement. This promising technique for cancer therapy show interesting effects on cancer cells *in vitro*. Nevertheless, more studies are needed to clearly identify the best parameters. A better understanding of cellular mechanisms involved could help to trigger specific pathways leading to cellular death. The induction of apoptosis – cell death mode particularly sought, minimizing adverse effects such as inflammation – is highlighted and its rate quantitatively evaluated in various studies.

Main advantages of TMMEP compared to other cancer therapy such as magnetic hyperthermia, surgery or pharmaco-therapies, could be less side effects and low invasiveness of the technique. TMMEP method is reported as appropriate for sparing the surrounding healthy cells, since the magneto-mechanical vibration applied on or within the targeted cancer cells remains highly local, in contrast with methods using heat which tends to diffuse into the neighboring tissues.[22,24]

Although these first trials of TMMEP treatments on cancer cells have yet to be deepened, the method could allow great improvements in future cancer treatments, and a hope for treating cancer with very poor prognosis as glioblastoma, for instance. Investigations on cancer cells destruction through magnetically actuated microparticles vibrating at low frequency, are finally of great interest for future cancer therapy, while remaining a big challenge. They will have to be pursued and deepened, in an effort to develop, on longer term, targeted cancer treatments with reduced side effects.

6. Conclusion–perspectives

The field of magneto-mechanical anti-cancer therapies has exponentially growth for the last 5 years, paving the foundation for new therapies in oncology. The main efficacy demonstration was done *in vitro*, using highly heterogeneous magnetic-responsive nanoparticles and magnetic stimulation. Beside the inaugural thermal effect, the demonstration that mechanical stimulation can modulate the cell biology of cancer is further comforted by the recent demonstration of mechano-transduction pathways. These pathways as well as the connected physico-mechanic properties of the tissues are probably as important for the physiological tissue homeostasis than the classical molecular pathways governing the initiation and promotion of cancer. Only a few *in vivo* investigations have been done, contrasting with the number of *in vitro* studies. *In vivo* strategies are confronted by the bottleneck of tissue delivery that is very poor after intravenous injection. Intratumor delivery is a growing alternative in nanomedicine that will be probably became the first strategy, increasing the efficacy of local nanoparticle delivery as well as it decreases the potential systemic side effects. Anticipating from the beginning of these investigations the biocompatibility of the nanoparticle is mandatory. Moreover, it will be also mandatory to decipher the physical properties of the targeted tissue, such as stiffness and intratissular pressure that could modulate the efficacy of magneto-mechanical therapy. Several imaging methodologies have been developed for that such as ultrasound stiffness imaging. A mechanical dosimetry mapping of the tissue should provide the opportunity of a real mechanical therapy personalization.

Both *in vitro* and *in vivo* studies in the field of magneto-mechanical therapies of cancer pave the way for a real renewing of cancer therapies, responding to the therapeutical resistances observed in the field of chemotherapy and targeted molecular and cellular therapies. Translating physics and nanomagnetism at the beside will need a strong interdisciplinarity associating synergistically physician, biologists and physicists.

Conflicts of interest

There are no conflicts to declare.

Acknowledgements

This work has been supported by funding from the European Union's H2020 ERA-Net EuroNanoMed II program Nanoviber Project – 16-ENM2-0008-02.

References

1 Q. A. Pankhurst, J. Connolly, S. K. Jones and J. P. Dobson, Applications of magnetic nanoparticles in biomedicine, *J. Phys. D: Appl. Phys.*, 2003, **36**, 167–181.
2 Y. Cheng, R. A. Morshed, B. Auffinger, A. L. Tobias and M. S. Lesniak, Multifunctional nanoparticles for brain tumor imaging and therapy, *Adv. Drug Delivery Rev.*, 2014, **66**, 42–57.
3 Z. R. Stephen, F. M. Kievit and M. Zhang, Magnetite nanoparticles for medical MR imaging, *Mater. Today*, 2011, **14**, 330–338.

4 R. Jin, B. Lin, D. Li and H. Ai, Superparamagnetic iron oxide nanoparticles for MR imaging and therapy: design considerations and clinical applications, *Curr. Opin. Pharmacol.*, 2014, **18**, 18–27.
5 M. Arruebo, R. Fernández-pacheco, M. R. Ibarra and J. Santamaría, Magnetic nanoparticles for drug delivery, *Nano Today*, 2007, **2**, 22–32.
6 V. V. Mody, A. Cox, S. Shah, A. Singh, W. Bevins and H. Parihar, Magnetic nanoparticle drug delivery systems for targeting tumor, *Appl. Nanosci.*, 2014, **4**, 385–392.
7 C. Sun, J. S. H. Lee and M. Zhang, Magnetic nanoparticles in MR imaging and drug delivery, *Adv. Drug Delivery Rev.*, 2008, **60**, 1252–1265.
8 O. L. Gobbo, K. Sjaastad, M. W. Radomski, Y. Volkov and A. Prina-Mello, Magnetic nanoparticles in cancer theranostics, *Theranostics*, 2015, **5**, 1249–1263.
9 Y. Gao, J. Lim, S.-H. Teoh and C. Xu, Emerging translational research on magnetic nanoparticles for regenerative medicine, *Chem. Soc. Rev.*, 2015, **44**, 6306–6329.
10 Q. Zhang, T. Yin, R. Xu, W. Gao, H. Zhao, J. G. Shapter, K. Wang, Y. Shen, P. Huang, G. Gao, Y. Wu and D. Cui, Large-scale immuno-magnetic cell sorting of T cells based on a self-designed high-throughput system for potential clinical application, *Nanoscale*, 2017, **9**, 13592–13599.
11 S. H. Cartmell, A. Keramane, G. R. Kirkham, S. B. Verschueren, J. L. Magnay, A. J. El Haj and J. Dobson, Use of magnetic particles to apply mechanical forces for bone tissue engineering purposes, *J. Phys.: Conf. Ser.*, 2005, **17**, 77–80.
12 J. L. Corchero and A. Villaverde, Biomedical applications of distally controlled magnetic nanoparticles, *Trends Biotechnol.*, 2009, **27**, 468–476.
13 C. Sanchez, D. El Hajj Diab, V. Connord, P. Clerc, E. Meunier, B. Pipy, B. Payré, R. P. Tan, M. Gougeon, J. Carrey, V. Gigoux and D. Fourmy, Targeting a G-protein-coupled receptor overexpressed in endocrine tumors by magnetic nanoparticles to induce cell death, *ACS Nano*, 2014, **8**, 1350–1363.
14 L. Kafrouni and O. Savadogo, Recent progress on magnetic nanoparticles for magnetic hyperthermia, *Prog. Biomater.*, 2016, **5**, 147–160.
15 S. Dutz and R. Hergt, Magnetic particle hyperthermia – a promising tumour therapy?, *Nanotechnology*, 2014, **25**, 1–28.
16 E. A. Vitol, V. Novosad and E. A. Rozhkova, Microfabricated magnetic structures for future medicine: from sensors to cell actuators, *Nanomedicine*, 2012, **7**, 1611–1624.
17 R. J. Mannix, S. Kumar, F. Cassiola, M. Montoya-Zavala, E. Feinstein, M. Prentiss and D. E. Ingber, Nanomagnetic actuation of receptor-mediated signal transduction, *Nat. Nanotechnol.*, 2008, **3**, 36–40.
18 S. Hughes, S. McBain, J. P. Dobson and A. J. El Haj, Selective activation of mechanosensitive ion channels using magnetic particles, *J. R. Soc., Interface*, 2008, **5**, 855–863.
19 A. O. Fung, V. Kapadia, E. Pierstorff, D. Ho and Y. Chen, Induction of cell death by magnetic actuation of nickel nanowires internalized by fibroblasts, *J. Phys. Chem. C*, 2008, **112**, 15085–15088.
20 V. Connord, P. Clerc, N. Hallali, D. El Hajj Diab, D. Fourmy, V. Gigoux and J. Carrey, Real-time analysis of magnetic hyperthermia experiments on living cells under a confocal microscope, *Small*, 2015, **11**, 2437–2445.
21 M. Domenech, I. Marrero-Berrios, M. Torres-Lugo and C. Rinaldi, Lysosomal membrane permeabilization by targeted magnetic nanoparticles in alternating magnetic fields, *ACS Nano*, 2013, **7**, 5091–5101.
22 D.-H. Kim, E. A. Rozhkova, I. V Ulasov, S. D. Bader, T. Rajh, M. S. Lesniak and V. Novosad, Biofunctionalized magnetic-vortex microdiscs for targeted cancer-cell destruction, *Nat. Mater.*, 2010, **9**, 165–171.
23 V. Novosad and E. A. Rozhkova, Ferromagnets-Based Multifunctional Nanoplatform for Targeted Cancer Therapy, in *Biomedical Engineering, Trends in Materials Science*, 2011, pp. 425–444.
24 M. Goiriena-Goikoetxea, D. Muñoz, I. Orue, M. L. Fernández-Gubieda, J. Bokor, A. Muela and A. García-Arribas, Disk-shaped magnetic particles for cancer therapy, *Appl. Phys. Rev.*, 2020, **7**, 011306.
25 M. Chen, J. Wu, P. Ning, J. Wang, Z. Ma, L. Huang, G. R. Plaza, Y. Shen, C. Xu, Y. Han, M. S. Lesniak, Z. Liu and Y. Cheng, Remote Control of Mechanical Forces via Mitochondrial-Targeted Magnetic Nanospinners for Efficient Cancer Treatment, *Small*, 2020, **16**, 1905424.
26 N. Maniotis, A. Makridis, E. Myrovali, A. Theopoulos, T. Samaras and M. Angelakeris, Magneto-mechanical action of multimodal field configurations on magnetic nanoparticle environments, *J. Magn. Magn. Mater.*, 2019, **470**, 6–11.
27 R. Mansell, T. Vemulkar, D. C. M. C. Petit, Y. Cheng, J. Murphy, M. S. Lesniak and R. P. Cowburn, Magnetic particles with perpendicular anisotropy for mechanical cancer cell destruction, *Sci. Rep.*, 2017, **7**, 1–7.
28 H. Ye, Z. Shen, L. Yu, M. Wei and Y. Li, Manipulating nanoparticle transport within blood flow through external forces: An exemplar of mechanics in nanomedicine, *Proc. R. Soc. A*, 2018, **474**, 1–24.
29 B. Wang, C. Bienvenu, J. Mendez-Garza, P. Lançon, A. Madeira, P. Vierling, C. Di Giorgio and G. Bossis, Necrosis of HepG2 cancer cells induced by the vibration of magnetic particles, *J. Magn. Magn. Mater.*, 2013, **344**, 193–201.
30 Y. Shen, C. Wu, T. Q. P. Uyeda, G. R. Plaza, B. Liu, Y. Han, M. S. Lesniak and Y. Cheng, Elongated nanoparticle aggregates in cancer cells for mechanical destruction with low frequency rotating magnetic field, *Theranostics*, 2017, **7**, 1735–1748.
31 D. Liu, L. Wang, Z. Wang and A. Cuschieri, Magnetoporation and magnetolysis of cancer cells via carbon nanotubes induced by rotating magnetic fields, *Nano Lett.*, 2012, **12**, 5117–5121.
32 D. Cheng, X. Li, G. Zhang and H. Shi, Morphological effect of oscillating magnetic nanoparticles in killing tumor cells, *Nanoscale Res. Lett.*, 2014, **9**, 1–8.
33 M. F. Contreras, R. Sougrat, A. Zaher, T. Ravasi and J. Kosel, Non-chemotoxic induction of cancer cell death using magnetic nanowires, *Int. J. Nanomed.*, 2015, **10**, 2141–2153.

34 D. Kilinc, A. Lesniak, S. A. Rashdan, D. Gandhi, A. Blasiak, P. C. Fannin, A. von Kriegsheim, W. Kolch and G. U. Lee, Mechanochemical Stimulation of MCF7 Cells with Rod-Shaped Fe–Au Janus Particles Induces Cell Death Through Paradoxical Hyperactivation of ERK, *Adv. Healthcare Mater.*, 2015, **4**, 395–404.

35 A. I. Martínez-Banderas, A. Aires, F. J. Teran, J. E. Perez, J. F. Cadenas, N. Alsharif, T. Ravasi, A. L. Cortajarena and J. Kosel, Functionalized magnetic nanowires for chemical and magneto-mechanical induction of cancer cell death, *Sci. Rep.*, 2016, **6**, 1–11.

36 D. W. Wong, W. L. Gan, N. Liu and W. S. Lew, Magneto-actuated cell apoptosis by biaxial pulsed magnetic field, *Sci. Rep.*, 2017, **7**, 1–8.

37 Y. Cheng, M. E. Muroski, D. C. M. C. Petit, R. Mansell, T. Vemulkar, R. A. Morshed, Y. Han, I. V. Balyasnikova, C. M. Horbinski, X. Huang, L. Zhang, R. P. Cowburn and M. S. Lesniak, Rotating magnetic field induced oscillation of magnetic particles for in vivo mechanical destruction of malignant glioma, *J. Controlled Release*, 2016, **223**, 75–84.

38 S. Leulmi, X. Chauchet, M. Morcrette, G. Ortiz, H. Joisten, P. Sabon, T. Livache, Y. Hou, M. Carrière, S. Lequien and B. Dieny, Triggering the apoptosis of targeted human renal cancer cells by the vibration of anisotropic magnetic particles attached to the cell membrane, *Nanoscale*, 2015, **7**, 15904–15914.

39 M. E. Muroski, R. A. Morshed, Y. Cheng, T. Vemulkar, R. Mansell, Y. Han, L. Zhang, K. S. Aboody, R. P. Cowburn and M. S. Lesniak, Controlled payload release by magnetic field triggered neural stem cell destruction for malignant glioma treatment, *PLoS One*, 2016, 1–12.

40 T. N. Zamay, G. S. Zamay, I. V Belyanina, S. S. Zamay, V. V Denisenko, O. S. Kolovskaya, T. I. Ivanchenko, V. L. Grigorieva, I. V Garanzha, D. V Veprintsev, Y. E. Glazyrin, A. V Shabanov, V. Y. Prinz, V. A. Seleznev, A. E. Sokolov, V. S. Propenko, P. D. Kim, A. Gargaun, M. V Berezovski and A. S. Zamay, Noninvasive microsurgery using aptamer-functionalized magnetic microdisks for tumor cell eradication, *Nucleic Acid Ther.*, 2017, **27**, 105–114.

41 S.-H. Hu and X. Gao, Nanocomposites with Spatially Separated Functionalities for Combined Imaging and Magnetolytic Therapy, *J. Am. Chem. Soc.*, 2010, **132**, 7234–7237.

42 M. H. Cho, E. J. Lee, M. Son, J. H. Lee, D. Yoo, J. W. Kim, S. W. Park, J. S. Shin and J. Cheon, A magnetic switch for the control of cell death signalling in in vitro and in vivo systems, *Nat. Mater.*, 2012, **11**, 1038–1043.

43 E. Zhang, M. F. Kircher, M. Koch, L. Eliasson, S. N. Goldberg and E. Renström, Dynamic Magnetic Fields Remote-Control Apoptosis via Nanoparticle Rotation, *ACS Nano*, 2014, **8**, 3192–3201.

44 A. M. Master, P. N. Williams, N. Pothayee, N. Pothayee, R. Zhang, H. M. Vishwasrao, Y. I. Golovin, J. S. Riffle, M. Sokolsky and A. V. Kabanov, Remote actuation of magnetic nanoparticles for cancer cell selective treatment through cytoskeletal disruption, *Sci. Rep.*, 2016, **6**, 1–13.

45 F. Wo, R. Xu, Y. Shao, Z. Zhang, M. Chu, D. Shi and S. Liu, A multimodal system with synergistic effects of magneto-mechanical, photothermal, photodynamic and chemo therapies of cancer in graphene-quantum dot-coated hollow magnetic nanospheres, *Theranostics*, 2016, **6**, 485–500.

46 H. Ju, Y. Cui, Z. Chen, Q. Fu, M. Sun and Y. Zhou, Effects of combined delivery of extremely low frequency electromagnetic field and magnetic Fe_3O_4 nanoparticles on hepatic cell lines, *Am. J. Transl. Res.*, 2016, **8**, 1838–1847.

47 R. Brossel, A. Yahi, S. David, L. Moreno Velasquez and J.-M. Guinebretière, Mechanical Signals Inhibit Growth of a Grafted Tumor In Vivo: Proof of Concept, *PLoS One*, 2016, **11**, e0152885.

48 S. Hapuarachchige, Y. Kato, E. J. Ngen, B. Smith, M. Delannoy and D. Artemov, Non-temperature induced effects of magnetized iron oxide nanoparticles in alternating magnetic field in cancer cells, *PLoS One*, 2016, **11**, 1–12.

49 A. Vegerhof, E. A. Barnoy, M. Motiei, D. Malka, Y. Danan, Z. Zalevsky and R. Popovtzer, Targeted magnetic nanoparticles for mechanical lysis of tumor cells by low-amplitude alternating magnetic field, *Materials*, 2016, **9**, 1–12.

50 W. Li, Y. Liu, Z. Qian and Y. Yang, Evaluation of Tumor Treatment of Magnetic Nanoparticles Driven by Extremely Low Frequency Magnetic Field, *Sci. Rep.*, 2017, **7**, 1–9.

51 O. Lunov, M. Uzhytchak, B. Smolková, M. Lunova, M. Jirsa, N. M. Dempsey, A. L. Dias, M. Bonfim, M. Hof, P. Jurkiewicz, Y. Petrenko, Š. Kubinová and A. Dejneka, Remote actuation of apoptosis in liver cancer cells via magneto-mechanical modulation of iron oxide nanoparticles, *Cancers*, 2019, **11**, 1–20.

52 H. Chiriac, E. Radu, M. □ibu, G. Stoian, G. Ababei, L. Lăbu□că, D.-D. Herea and N. Lupu, Fe–Cr–Nb–B ferromagnetic particles with shape anisotropy for cancer cell destruction by magneto-mechanical actuation, *Sci. Rep.*, 2018, **8**, 1–9.

53 D. Ling and T. Hyeon, Chemical design of biocompatible iron oxide nanoparticles for medical applications, *Small*, 2013, **9**, 1450–1466.

54 M. Samadishadlou, M. Farshbaf, N. Annabi, T. Kavetskyy, R. Khalilov, S. Saghfi, A. Akbarzadeh and S. Mousavi, Magnetic carbon nanotubes: preparation, physical properties, and applications in biomedicine, *Artif. Cells, Nanomed., Biotechnol.*, 2018, **46**, 1314–1330.

55 S. Leulmi, H. Joisten, T. Dietsch, C. Iss, M. Morcrette, S. Auffret, P. Sabon and B. Dieny, Comparison of dispersion and actuation properties of vortex and synthetic antiferromagnetic particles for biotechnological applications, *Appl. Phys. Lett.*, 2013, **103**, 8–13.

56 M. Ermolli, C. Menné, G. Pozzi, M. ángel Serra and L. A. Clerici, Nickel, cobalt and chromium-induced cytotoxicity and intracellular accumulation in human HaCaT keratinocytes, *Toxicology*, 2001, **159**, 23–31.

57 E. C. Dreaden, A. M. Alkilany, X. Huang, C. J. Murphy and M. A. El-Sayed, The golden age: gold nanoparticles for biomedicine, *Chem. Soc. Rev.*, 2012, **41**, 2740–2779.

58 R. Shukla, V. Bansal, M. Chaudhary, A. Basu, R. R. Bhonde and M. Sastry, Biocompatibility of gold nanoparticles and their endocytotic fate inside the cellular compartment: a microscopic overview, *Langmuir*, 2005, **21**, 10644–10654.

59 H. Hartmann and R. Krastev, Biofunctionalization of surfaces using polyelectrolyte multilayers, *BioNanoMaterials*, 2017, 20160015, 12pp.
60 I. Bodhinayake, M. Ottenhausen and J. A. Boockvar, Targeting a heterogeneous tumor: The promise of the interleukin-13 receptor α2, *Neurosurgery*, 2014, **75**, 18–19.
61 C. G. Hadjipanayis, R. Machaidze, M. Kaluzova, L. Wang, A. J. Schuette, H. Chen, X. Wu and H. Mao, EGFRvIII antibody-conjugated iron oxide nanoparticles for magnetic resonance imaging-guided convection-enhanced delivery and targeted therapy of glioblastoma, *Cancer Res.*, 2010, **70**, 6303–6312.
62 E. Prats-Alfonso and F. Albericio, Functionalization of gold surfaces: recent developments and applications, *J. Mater. Sci.*, 2011, **46**, 7643–7648.
63 P. Decuzzi, B. Godin, T. Tanaka, S. Y. Lee, C. Chiappini, X. Liu and M. Ferrari, Size and shape effects in the biodistribution of intravascularly injected particles, *J. Controlled Release*, 2010, **141**, 320–327.
64 A. Albanese, P. S. Tang and W. C. W. Chan, The Effect of Nanoparticle Size, Shape, and Surface Chemistry on Biological Systems, *Annu. Rev. Biomed. Eng.*, 2012, **14**, 1–16.
65 H. Ye, Z. Shen and Y. Li, Computational modeling of magnetic particle margination within blood flow through LAMMPS, *Comput. Mech.*, 2018, **62**, 457–476.
66 S. Wilhelm, A. J. Tavares, Q. Dai, S. Ohta, J. Audet, H. F. Dvorak and W. C. W. Chan, Analysis of nanoparticle delivery to tumours, *Nat. Rev. Mater.*, 2016, **1**, 1–12.
67 Y. Geng, P. Dalhaimer, S. Cai, R. Tsai, M. Tewari, T. Minko and D. E. Discher, Shape effects of filaments versus spherical particles in flow and drug delivery, *Nat. Nanotechnol.*, 2007, **2**, 249–255.
68 E. Carboni, K. Tschudi, J. Nam, X. Lu and A. W. K. Ma, Particle margination and its implications on intravenous anticancer drug delivery, *AAPS PharmSciTech*, 2014, **15**, 762–771.
69 F. Gentile, A. Curcio, C. Indolfi, M. Ferrari and P. Decuzzi, The margination propensity of spherical particles for vascular targeting in the microcirculation, *J. Nanobiotechnol.*, 2008, **6**, 1–9.
70 V. P. Chauhan, Z. Popović, O. Chen, J. Cui, D. Fukumura, M. G. Bawendi and R. K. Jain, Fluorescent nanorods and nanospheres for real-time in vivo probing of nanoparticle shape-dependent tumor penetration, *Angew. Chem., Int. Ed.*, 2011, **50**, 11417–11420.
71 S. K. Hobbs, W. L. Monsky, F. Yuan, W. G. Roberts, L. Griffith, V. P. Torchilin and R. K. Jain, Regulation of transport pathways in tumor vessels: role of tumor type and microenvironment, *Proc. Natl. Acad. Sci. U. S. A.*, 1998, **95**, 4607–4612.
72 Q. Li, C. W. Kartikowati, S. Horie, T. Ogi, T. Iwaki and K. Okuyama, Correlation between particle size/domain structure and magnetic properties of highly crystalline Fe_3O_4 nanoparticles, *Sci. Rep.*, 2017, **7**, 1–4.
73 N. H. Hai, N. H. Luong, N. Chau and N. Q. Tai, Preparation of magnetic nanoparticles embedded in polystyrene microspheres, *J. Phys.: Conf. Ser.*, 2009, **187**, 1–6.
74 K. Hayashi, M. Nakamura, W. Sakamoto, T. Yogo, H. Miki, S. Ozaki, M. Abe, T. Matsumoto and K. Ishimura, Superparamagnetic nanoparticle clusters for cancer theranostics combining magnetic resonance imaging and hyperthermia treatment, *Theranostics*, 2013, **3**, 366–376.
75 S. Kralj and D. Makovec, Magnetic Assembly of Superparamagnetic Iron Oxide Nanoparticle Clusters into Nanochains and Nanobundles, *ACS Nano*, 2015, **9**, 9700–9707.
76 H. Joisten, T. Courcier, P. Balint, P. Sabon, J. Faure-Vincent, S. Auffret and B. Dieny, Self-polarization phenomenon and control of dispersion of synthetic antiferromagnetic nanoparticles for biological applications, *Appl. Phys. Lett.*, 2010, **97**, 2–4.
77 K. Y. Guslienko, V. Novosad, Y. Otani, H. Shima and K. Fukamichi, Field evolution of magnetic vortex state in ferromagnetic disks, *Appl. Phys. Lett.*, 2001, **78**, 3848–3850.
78 W. Hu, R. J. Wilson, A. Koh, A. Fu, A. Z. Faranesh, C. M. Earhart, S. J. Osterfeld, S. J. Han, L. Xu, S. Guccione, R. Sinclair and S. X. Wang, High-moment antiferromagnetic nanoparticles with tunable magnetic properties, *Adv. Mater.*, 2008, **20**, 1479–1483.
79 T. Vemulkar, R. Mansell, D. C. M. C. Petit, R. P. Cowburn and M. S. Lesniak, Highly tunable perpendicularly magnetized synthetic antiferromagnets for biotechnology applications, *Appl. Phys. Lett.*, 2015, **107**, 012403.
80 E. A. Rozhkova, V. Novosad, D.-H. Kim, J. Pearson, R. Divan, T. Rajh and S. D. Bader, Ferromagnetic microdisks as carriers for biomedical applications, *J. Appl. Phys.*, 2009, **105**, 58–61.
81 M. Goiriena-Goikoetxea, A. García-Arribas, M. Rouco, A. V. Svalov and J. M. Barandiaran, High-yield fabrication of 60 nm permalloy nanodiscs in well-defined magnetic vortex state for biomedical applications, *Nanotechnology*, 2016, **27**, 175302.
82 Y. P. Ivanov, M. Vázquez and O. Chubykalo-Fesenko, Magnetic reversal modes in cylindrical nanowires, *J. Phys. D: Appl. Phys.*, 2013, **46**, 11pp.
83 H. Joisten, A. Truong, S. Ponomareva, C. Naud, R. Morel, Y. Hou, I. Joumard, S. Auffret, P. Sabon and B. Dieny, Optical response of magnetically actuated biocompatible membranes, *Nanoscale*, 2019, **11**, 10667–10683.
84 M. Morcrette, *Micro et nanoparticules pour des applications biotechnologiques: fabrication de nanoparticules par copolymère dibloc pour l'imagerie médicale; destruction de cellules cancéreuses par vibrations magnéto- mécaniques de microparticules magnétiques*, PhD thesis, Univ. Grenoble Alpes, 2015, https://www.theses.fr/2015GREAY052.
85 Y. Chen, L. Ju, M. Rushdi, C. Ge and C. Zhu, Receptor-mediated cell mechanosensing, *Mol. Biol. Cell*, 2017, 3134–3155.
86 L. Galluzzi, I. Vitale, S. A. Aaronson, J. M. Abrams, D. Adam, P. Agostinis, E. S. Alnemri, L. Altucci, I. Amelio, D. W. Andrews, M. Annicchiarico-Petruzzelli, A. V. Antonov, E. Arama, E. H. Baehrecke, N. A. Barlev, N. G. Bazan, F. Bernassola, M. J. M. Bertrand, K. Bianchi, M. V. Blagosklonny, K. Blomgren, C. Borner, P. Boya,

C. Brenner, M. Campanella, E. Candi, D. Carmona-Gutierrez, F. Cecconi, F. K. M. Chan, N. S. Chandel, E. H. Cheng, J. E. Chipuk, J. A. Cidlowski, A. Ciechanover, G. M. Cohen, M. Conrad, J. R. Cubillos-Ruiz, P. E. Czabotar, V. D'Angiolella, T. M. Dawson, V. L. Dawson, V. De Laurenzi, R. De Maria, K. M. Debatin, R. J. Deberardinis, M. Deshmukh, N. Di Daniele, F. Di Virgilio, V. M. Dixit, S. J. Dixon, C. S. Duckett, B. D. Dynlacht, W. S. El-Deiry, J. W. Elrod, G. M. Fimia, S. Fulda, A. J. García-Sáez, A. D. Garg, C. Garrido, E. Gavathiotis, P. Golstein, E. Gottlieb, D. R. Green, L. A. Greene, H. Gronemeyer, A. Gross, G. Hajnoczky, J. M. Hardwick, I. S. Harris, M. O. Hengartner, C. Hetz, H. Ichijo, M. Jäättelä, B. Joseph, P. J. Jost, P. P. Juin, W. J. Kaiser, M. Karin, T. Kaufmann, O. Kepp, A. Kimchi, R. N. Kitsis, D. J. Klionsky, R. A. Knight, S. Kumar, S. W. Lee, J. J. Lemasters, B. Levine, A. Linkermann, S. A. Lipton, R. A. Lockshin, C. López-Otín, S. W. Lowe, T. Luedde, E. Lugli, M. MacFarlane, F. Madeo, M. Malewicz, W. Malorni, G. Manic, J. C. Marine, S. J. Martin, J. C. Martinou, J. P. Medema, P. Mehlen, P. Meier, S. Melino, E. A. Miao, J. D. Molkentin, U. M. Moll, C. Muñoz-Pinedo, S. Nagata, G. Nuñez, A. Oberst, M. Oren, M. Overholtzer, M. Pagano, T. Panaretakis, M. Pasparakis, J. M. Penninger, D. M. Pereira, S. Pervaiz, M. E. Peter, M. Piacentini, P. Pinton, J. H. M. Prehn, H. Puthalakath, G. A. Rabinovich, M. Rehm, R. Rizzuto, C. M. P. Rodrigues, D. C. Rubinsztein, T. Rudel, K. M. Ryan, E. Sayan, L. Scorrano, F. Shao, Y. Shi, J. Silke, H. U. Simon, A. Sistigu, B. R. Stockwell, A. Strasser, G. Szabadkai, S. W. G. Tait, D. Tang, N. Tavernarakis, A. Thorburn, Y. Tsujimoto, B. Turk, T. Vanden Berghe, P. Vandenabeele, M. G. Vander Heiden, A. Villunger, H. W. Virgin, K. H. Vousden, D. Vucic, E. F. Wagner, H. Walczak, D. Wallach, Y. Wang, J. A. Wells, W. Wood, J. Yuan, Z. Zakeri, B. Zhivotovsky, L. Zitvogel, G. Melino and G. Kroemer, Molecular mechanisms of cell death: recommendations of the Nomenclature Committee on Cell Death 2018, *Cell Death Differ.*, 2018, **25**, 486–541.

87 I. K. H. Poon, C. D. Lucas, A. G. Rossi and K. S. Ravichandran, Apoptotic cell clearance: basic biology and therapeutic potential, *Nat. Rev. Immunol.*, 2014, **14**, 166–180.

88 Z. Jin and W. S. El-Deiry, Overview of cell death signaling pathways, *Cancer Biol. Ther.*, 2005, **4**, 147–171.

89 G. Liu, C. Wu, Y. Wu and Y. Zhao, Phagocytosis of Apoptotic Cells and Immune Regulation, *Scand. J. Immunol.*, 2006, **64**, 1–9.

90 M. Desouza, P. W. Gunning and J. R. Stehn, The actin cytoskeleton as a sensor and mediator of apoptosis, *Bioarchitecture*, 2012, **2**, 75–87.

91 R. M. Mohammada, I. Muqbil, L. Lowe, C. Yedjou, H.-Y. Hsu, L.-T. Lin, M. D. Siegelin, C. Fimognari, N. B. Kumar, Q. P. Dou, H. Yang, A. K. Samadi, G. L. Russo, C. Spagnuolo, S. K. Ray, M. Chakrabarti, J. D. Morre, H. M. Coley, K. Honoki, H. Fujii, A. G. Georgakila, A. Amedei, E. Niccolai, A. Amin, S. S. Ashraf, W. G. Helferich, X. Yang, C. S. Boosani, G. Guha, D. Bhakta, M. R. Ciriolo, K. Aquilano, S. Chen, S. I. Mohammed, W. N. Keith, A. Bilsland, D. Halicka, S. Nowsheen and A. S. Azmi, Broad targeting of resistance to apoptosis in cancer, *Semin. Cancer Biol.*, 2015, **35**, 1–63.

92 A. Kroll, M. H. Pillukat, D. Hahn and J. Schnekenburger, Interference of engineered nanoparticles with in vitro toxicity assays, *Arch. Toxicol.*, 2012, **86**, 1123–1136.

93 K. J. Ong, T. J. MacCormack, R. J. Clark, J. D. Ede, V. A. Ortega, L. C. Felix, M. K. M. Dang, G. Ma, H. Fenniri, J. G. C. Veinot and G. G. Goss, Widespread Nanoparticle-Assay Interference: Implications for Nanotoxicity Testing, *PLoS One*, 2014, **9**, e90650 1–9.

94 N. Kavčič, K. Pegan and B. Turk, Lysosomes in programmed cell death pathways: from initiators to amplifiers, *Biol. Chem.*, 2017, **398**, 289–301.

95 A. M. Villamil Giraldo, H. Appelqvist, T. Ederth and K. Öllinger, Lysosomotropic agents: impact on lysosomal membrane permeabilization and cell death, *Biochem. Soc. Trans.*, 2014, **42**, 1460–1464.

96 C. W. Gourlay and K. R. Ayscough, The actin cytoskeleton: a key regulator of apoptosis and ageing?, *Nat. Rev. Mol. Cell Biol.*, 2005, **6**, 583–589.

97 J. P. Dobson, Remote control of cellular behaviour with magnetic nanoparticles, *Nat. Nanotechnol.*, 2008, **3**, 139–143.

98 F. Broders-Bondon, T. H. N. Ho-Bouldoires, M. E. Fernandez-Sanchez and E. Farge, Mechanotransduction in tumor progression: the dark side of the force, *J. Cell Biol.*, 2018, **217**, 1571–1587.

99 D. D. Vo, R. M. Prins, J. L. Begley, T. R. Donahue, L. F. Morris, K. W. Bruhn, P. de la Rocha, M.-Y. Yang, S. Mok, H. J. Garban, N. Craft, J. S. Economou, F. M. Marincola, E. Wang and A. Ribas, Enhanced Antitumor Activity Induced by Adoptive T-Cell Transfer and Adjunctive Use of the Histone Deacetylase Inhibitor LAQ824, *Cancer Res.*, 2009, **69**, 8693–8699.

100 T. Klei, F. Souza, M. P. Nucci, J. B. Mamani, R. Silva, D. Maciely, C. Fantacini, L. E. B. De, V. Picanc, D. T. Covas, E. L. Vidoto, T. K. Felix Souza, M. P. Nucci, J. B. Mamani, H. Rodrigues da Silva, D. M. Carvalho Fantacini, L. E. Botelho de Souza, V. Picanço-Castro, D. T. Covas, E. L. Vidoto, A. Tannús and L. F. Gamarra, Image and motor behavior for monitoring tumor growth in C6 glioma model, *PLoS One*, 2018, **13**, 1–21.

101 C. Naud, *Particules magnétiques pour le traitement du cancer par effet magnéto-mécanique, application au glioblastome*, PhD thesis, Université Grenoble Alpes, 2019, http://www.theses.fr/2019GREAS005.

102 C. Naud, A 3D spheroid-based model for preclinical evaluation of treatment by magneto mechanical effect of particles in cancer therapy, to be publ.

103 S. Rebouissou, J. Zucman-Rossi, R. Moreau, Z. Qiu and L. Hui, Note of caution: contaminations of hepatocellular cell lines, *J. Hepatol.*, 2017, **67**, 896–897.